

## Article

# Strain Analysis and Kinematics of Deformation of the Tectonic Nappe Pile in Olympos-Ossa Mountainous Area: Implication for the Exhumation History of the HP/LT Ampelakia Unit and the Olympos-Ossa Tectonic Window (Eastern Thessaly, Central Greece)

Ioannis Vrontzos <sup>1</sup>, Emmanouil Katrivanos <sup>1</sup> , Ilias Lazos <sup>2,\*</sup> , Lambrini Papadopoulou <sup>1</sup>  and Adamantios Kiliias <sup>1</sup>

<sup>1</sup> School of Geology, Department of Geology, Aristotle University Thessaloniki, 54124 Thessaloniki, Greece; vrontzos@geo.auth.gr (I.V.); ekatriva@geo.auth.gr (E.K.); lambrini@geo.auth.gr (L.P.); kiliias@geo.auth.gr (A.K.)

<sup>2</sup> School of Mineral Resources Engineering, Technical University of Crete, 73100 Chania, Greece

\* Correspondence: ilazos@tuc.gr; Tel.: +30-2821037652

**Abstract:** This paper focuses on the structural and finite strain analysis of the Pelagonian nappe, the HP/LT Ampelakia unit, and the Olympos-Ossa unit in the Olympos-Ossa mountainous area in order to better understand the exhumation history of the Ampelakia unit and the underlain Olympos-Ossa unit. Two main stages of Tertiary deformation were revealed, related to nappe stacking and exhumation processes. During the Paleocene–Eocene crustal subduction, HP/LT metamorphism, compression, and nappe stacking were developed progressively. This D<sub>1</sub> stage was terminated with the final SW-ward emplacement of the Ampelakia and Pelagonian nappe on the Olympos-Ossa unit during the Eocene–Early Oligocene. The next stage of deformation, D<sub>2</sub>, was developed during the Oligocene–Miocene following the orogenic nappes stacking. D<sub>2</sub> was considered an extensional event, related to metamorphic isothermal decompression, nappes tectonic denudation, crustal uplift, and final exhumation of the Ampelakia unit and the Olympos-Ossa unit as a tectonic window. The calculated finite strain ellipsoids indicate a main flattening type strain geometry and middle strain intensity, increasing along the nappe contacts. The quartz C-axes diagrams also reveal a flattening type of deformation and non-coaxial flow towards the southwest and northeast at the western and eastern flanks of Olympos-Ossa Mountain, respectively. The calculated  $W_k$  vorticity number ranges from 0.23 to 0.93.

**Keywords:** blueschists; nappes stacking; exhumation; extrusion wedge; strain analysis; detachment faults



**Citation:** Vrontzos, I.; Katrivanos, E.; Lazos, I.; Papadopoulou, L.; Kiliias, A. Strain Analysis and Kinematics of Deformation of the Tectonic Nappe Pile in Olympos-Ossa Mountainous Area: Implication for the Exhumation History of the HP/LT Ampelakia Unit and the Olympos-Ossa Tectonic Window (Eastern Thessaly, Central Greece). *Geosciences* **2024**, *14*, 179. <https://doi.org/10.3390/geosciences14070179>

Academic Editors: Jesus Martinez-Frias and Ian Alsop

Received: 1 June 2024

Revised: 21 June 2024

Accepted: 24 June 2024

Published: 28 June 2024



**Copyright:** © 2024 by the authors. Licensee MDPI, Basel, Switzerland. This article is an open access article distributed under the terms and conditions of the Creative Commons Attribution (CC BY) license (<https://creativecommons.org/licenses/by/4.0/>).

## 1. Introduction

Our study area includes the Olympos-Ossa mountainous area, which is part of the Hellenides and is located in the central part of the Greek mainland (Figure 1). The complicated tectonics is the main feature of this region, as several compressional (nappes stacking, thrust faults, and crustal thickening) and extensional (nappes denudation, normal detachment faults, and crustal exhumation) tectonic events are documented ([1] and references therein), while its major highlight is the HP/LT rock formations constituting the Ampelakia unit. This tectonic setting complexity has raised queries about the structural evolution of this area, in which the Ampelakia unit plays a key role. What is the direction of the nappe's movement and the quantitative and qualitative characteristics of deformation? What kind of emplacement mechanism was performed at the HP/LT Ampelakia unit, and which is the corresponding one for the crustal exhumation and formation of the Olympos-Ossa window? Which is the best interpretation model of the structural and geotectonic evolution of the

Olympos-Ossa area? Additionally, this region is notable for the exposure of high-pressure rocks that were subducted at great depth, metamorphosed to blueschist-facies metamorphic conditions, and subsequently exhumed without being overprinted by higher-temperature metamorphic assemblages. Therefore, our study is focused on the determination of the early and final exhumation mechanisms of the Ampelakia unit and the Olympos-Ossa tectonic window, simultaneously highlighting the related controversial views, in order to comprehend the structural evolution of this area.

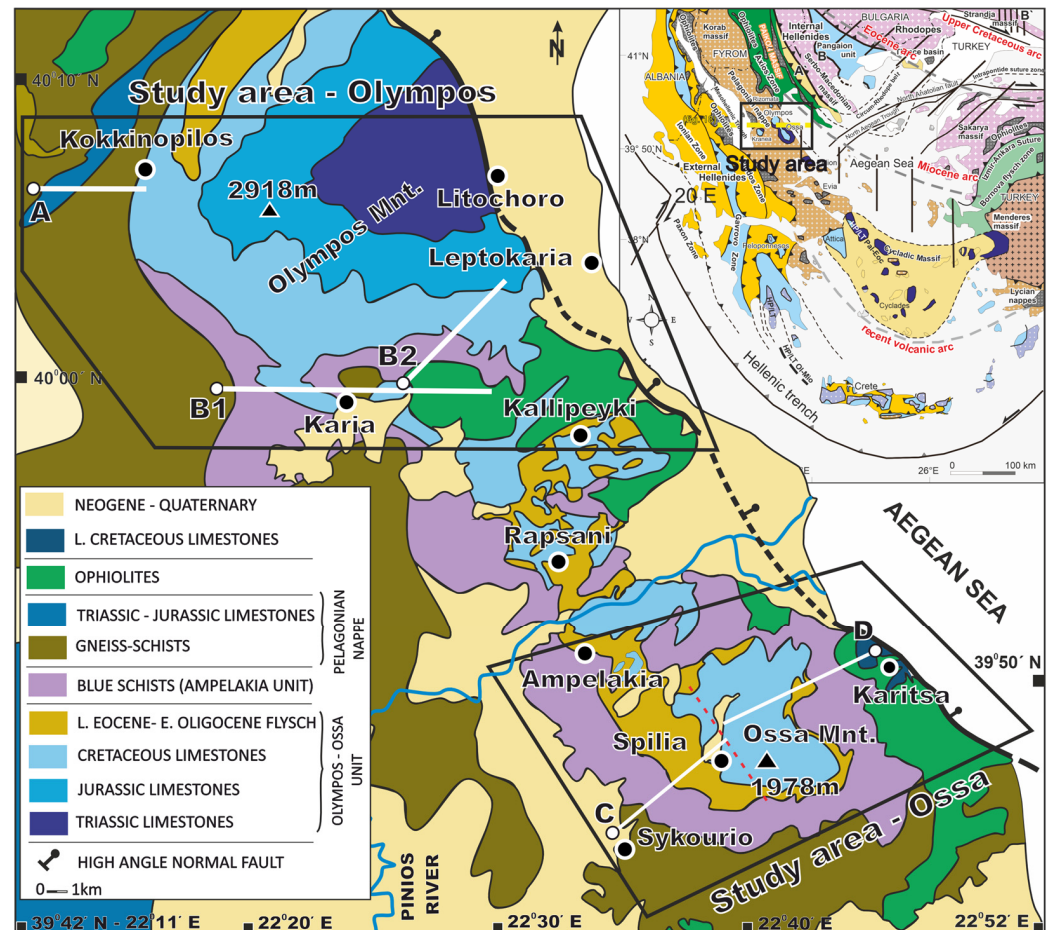


**Figure 1.** Simplified geological map showing the main structural domains of the Olympos-Ossa mountainous area (modified after [2–5]). Insert: Geological map of the Hellenides with the main structural domains and their continuation to the adjacent orogenic belts [1].

Regarding structural geology, the Olympos-Ossa mountainous area is formed by a complicated tectonic nappes pile consisting of continental and oceanic crust rocks, which are (from the uppermost to the lowermost): the Axios ophiolites, the Pelagonian nappe, the HP/LT Ampelakia unit, and the Olympos-Ossa unit. Focusing on the HP/LT Ampelakia unit, it was metamorphosed during the Paleocene–Eocene, under HP/LT metamorphic conditions, representing nowadays the suture zone between the Pelagonian nappe pile (Internal Hellenides) and the External Hellenides (Figure 1; [2,6–10]). These blueschist rocks, which characterize this unit, expand to the south in Evia Island and Cyclades, forming an arcuate-type HP belt [1,3,9,11–14].

Detailed studies in the adjacent Evia and Cyclades areas [11,12,15–18] concluded that there is strong evidence of an extrusion wedge that affects the early exhumation of HP units. This extrusion wedge is related to a potential NE-ward normal fault motion at the top and a SW-ward thrust fault motion at the base, respectively. According to Lister & Forster [19], a mechanism of large-scale detachment faults is responsible for the exhumation of the HP

unit of the Cycladic area. Other studies suggest that the exhumation of the HP unit in the Pelion area occurred due to a retroward ENE-directed ductile extrusion [3,20–25].

Furthermore, several researchers [2,9,10,14,26] support that the HP/LT Ampelakia unit, as well as the Pelagonian nappe were emplaced SW-ward above the Olympos-Ossa unit during the Eocene–Early Oligocene. Some authors [8,27,28] mention that the Paleocene–Eocene blueschist-facies structures of the Aegean region, related to crustal shortening and nappe stacking, escape exacted documentation due to the strong overprint effect of the later extensional deformation stage.

As a result, this paper focuses on (i) explaining the structural and strain analysis of the Olympos-Ossa area nappes pile, (ii) providing a better comprehension of the emplacement direction and the exhumation processes of the HP/LT Ampelakia unit and the Olympos-Ossa window, and (iii) contributing to the interpretation of the geotectonic evolution of the Hellenides.

## 2. Geological Setting

Plate tectonics in the eastern part of the Mediterranean region have produced a complicated geodynamic setting: the Anatolian microplate's tectonic escape to the west pushes the corresponding Aegean southwestward, resulting in powerful intraplate deformation manifested in large tectonic structures, while this deformation resulted in the formation of numerous crustal faults [29,30]. The two main intraplate features linked to the high seismic activity are the North Anatolian Fault Zone (NAFZ) and the Hellenic Subduction Zone (HSZ), sometimes referred to as the Hellenic Arc. The 80-million-year development of the Hellenic Arc, which moved southward to its present location as the subducting slab simultaneously rolled back, is the main characteristic of Aegean geodynamics [31,32]. Due to the westward prolongation (North Aegean Trough—NAT) of the North Anatolian Fault (NAF) into the North Aegean Sea, the Anatolian plate pushed the Aegean southwestward; this process led to the creation of a complicated seismotectonic regime across the eastern part of the Aegean Sea. Previous research (e.g., [29,33]) indicates that since the Eocene–Miocene, the Hellenic Trench has retreated (about 580 km) [34,35]. The Aegean and Anatolian areas exhibit N–S and NE–SW extensional occurrences as a result of these geological phenomena, which have given rise to a tectonic regime [36]. The occurrences of pull and push generated by the HSZ forces appear to be connected to the southwest Anatolian microplate motion [31], while the thickness of the lithosphere in the Aegean region is being influenced by this movement [37]. The thinning of the upper crust, documented in central and northern Greece, is caused by the extensional stress field generated by the Hellenic Trench (HT) retreat [38,39].

Focusing on the study area, the Olympos-Ossa mountain mass belongs to the Eastern Thessaly—Central Greece region (Figure 1) and is characterized by a complex tectonic nappes pile, which was successively formed from the Jurassic to the Tertiary, through alternating compressional and extensional tectonic events, causing nappe stacking and crustal uplift, respectively [1–3,6,7,9,10,14].

In particular, this nappes pile (Figure 2) consists of (from the uppermost to the lowermost): I. The Neotethyan ophiolites. They were obducted during the Middle-Late Jurassic on the Pelagonian Triassic-Jurassic platform carbonate cover. Late Cretaceous shallow water limestone overlies transgressively the ophiolites, which evolved to a Late Cretaceous-Paleocene flysch deposition [40–45]. II. The Pelagonian nappe. It is composed of a Paleozoic or older poly-metamorphic basement, overlain by a low-grade metamorphic volcano-sedimentary Permo-Triassic series and Triassic-Jurassic recrystallized carbonate cover. The Paleozoic crystalline basement consists of mica schists, amphibole schists, amphibolites, and para- and ortho-gneisses, intruded by calc-alkaline carboniferous (ca. 300 Ma) granitoids [2,46–50]. The Pelagonian basement has been affected by an HP metamorphism > 150 Ma, a retrograde amphibolite to greenschist facies metamorphism of Late Jurassic–Early Cretaceous age, and a Late–Early Cretaceous greenschist facies metamorphism. A residual Hercynian metamorphism has also been described [48,50–52]. III.

The Ampelakia unit. It was metamorphosed during the Paleocene–Eocene under HP/LT conditions, (pressure up to 6–7 Kbar and temperature around 400–480 °C), due to subduction under the Pelagonia, and subsequently affected by retrograde greenschist faces metamorphism during the Oligocene–Miocene. The Ampelakia unit has been identified as a volcano-sedimentary series (of unknown origin) consisting of metabasites and meta-sediment intercalations [2,8–10,53]. The Ampelakia unit is tectonically emplaced on the lowermost Olympos-Ossa Unit, along with the Pelagonian nappes pile, during the Eocene–Early Oligocene [2,3,8–10,54,55]. IV. The Olympos-Ossa unit. It consists of a thick carbonate unit deposited in a neritic environment on the Apulian passive continental margin without stratigraphic gaps from the Triassic to the Eocene. This series was completed with the deposition of a Late Eocene–Early Oligocene flysch formation. This unit is mentioned as a part of the External Hellenides carbonate Gavrovo zone exhumed as a tectonic window below the HP Ampelakia unit and the Pelagonian nappe during the Oligocene–Miocene [2,3,9,10,14,26].

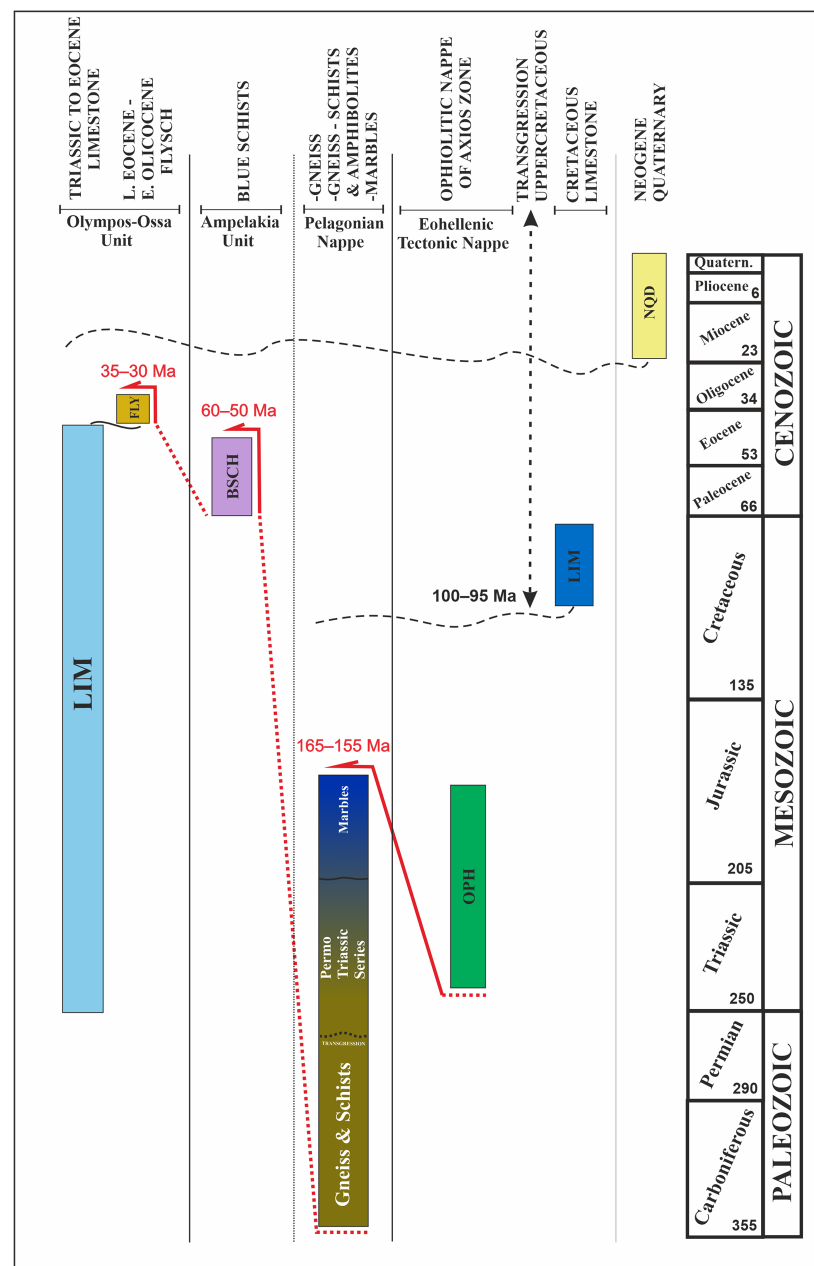


Figure 2. The tectonostratigraphic column of the Olympos-Ossa area (not in scale).

### 3. Results

#### 3.1. Structural Analysis

Field and laboratory surveys were carried out, utilizing geological/structural mapping, as well as modern methods for the strain and kinematics of deformation analysis, to ascertain the structural evolution of the study area [56–58].

Therefore, for this purpose, many oriented samples were collected from the Olympos-Ossa unit, Ampelakia unit, and Pelagonian nappe for micro-fabric analysis, enabling the establishment of the deformation regime and tectonic history of this area. Our survey distinguishes two main tectonic events, confirmed by previous researches (e.g., [4,8,10,14,26,45]).

The structures of the first  $D_1$  tectonic event were mainly documented in the Ampelakia unit and the deeper parts of the Pelagonian basement. They are relict and characterized by isoclinal, recumbent, usually intrafoliate folds, subparallel to an  $L_1$  stretching lineation, which is preserved on the  $S_1$  schistosity planes.

On sites where the  $D_1$  event is documented, the  $L_1$  lineation is mainly created by the parallel development of blue amphiboles (Figure 3j; glaucophane), white micas (phengite), epidote, elongated quartz, and albite. The syn- $D_1$  metamorphic mineral paragenesis (glaucophane, albite, lawsonite, chlorite, and quartz) shows that the  $D_1$  tectonic event took place under HP/LT metamorphic conditions. It was developed during compression and NE-ward subduction plunge of the Ampelakia unit under the Pelagonian nappe pile during the Paleocene–Eocene [1,2,6,7,9,10,14,55].

No clear shear sense kinematic indicators and structures of the  $D_1$  event are saved because it is strongly replaced by the second deformation,  $D_2$  (Figure 3i). During the progressive stages of the  $D_1$  event, nappe stacking takes place, associated with the WSW-ward (Figure 3j) final emplacement of the Ampelakia unit and Pelagonian nappe pile onto the carbonate Olympos-Ossa unit during the Eocene–Early Oligocene, as has also been mentioned by Schermer [6,9], Schermer et al. [7], Kiliass [1,10,14,55], and Kiliass et al. [8,26]. W-SW-ward overthrusting is in agreement with an E-NE-ward dipping of subduction of the Ampelakia unit under the Pelagonian nappe, proposed by Godfriaux [2], Schermer [6,9], Schermer et al. [7], Kiliass [1,10,14,55] and Kiliass et al. [8,26].

The second tectonic event,  $D_2$ , is the dominant ductile tectonic event in the study area and is characterized by a penetrative, mylonitic  $S_2$  schistosity (Figure 3), as well as by a NE-SW-trending  $L_2$  stretching lineation, imprinted on the  $S_2$  planes. Sub-isoclinal and sheath folds are also developed during the  $D_2$  and are similarly parallel, evolved to the  $L_2$  stretching lineation (Figure 3).

$S_2$  shows a SW-ward dip-direction at the western flank of the Olympos-Ossa mountainous area and a NE-ward one at the eastern mountainous flank, respectively (Figures 3 and 4). The  $L_2$  stretching lineation follows the same structural geometry with the  $S_2$  schistosity planes, plunging SW-ward and NE-ward at the western and eastern flanks of the Olympos-Ossa mountainous area, respectively. The  $D_2$  has strongly affected all tectonic units of the study nappe stack, which, from the bottom to the top, are: The Olympos-Ossa unit, the Ampelakia unit, and at least the deeper parts of the Pelagonian basement.

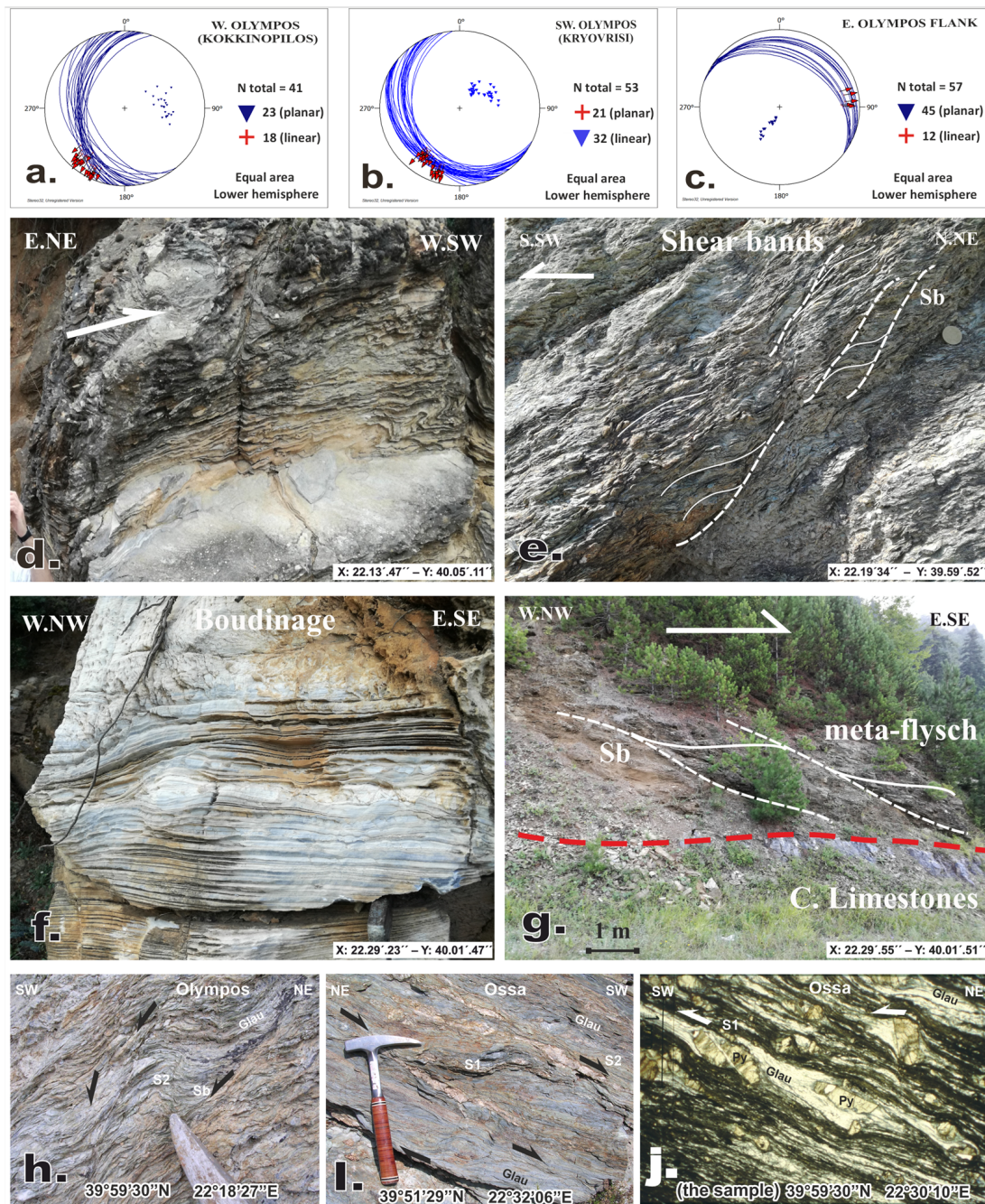


**Figure 3.** (a–c) Schmidt diagrams: Projection of the  $S_2$  foliation and  $L_2$  stretching lineation (equal area lower hemisphere), at the western (Kokkinopilos village), south-western (Kryovrisi village), and eastern flanks of the Olympos region, respectively. The arrows indicate the plunge of stretching lineation. (d–g) Structures and kinematic indicators of the Olympos region: At the western flank: (d) Sub-isoclinal asymmetric folds during  $D_2$  (carbonate of the Olympos-Ossa unit), (e) Shear bands, indicating a WSW-ward sense of movement (Pelagonian schist-gneisses). At the eastern flank: (f) Boudinage structures (Olympos-Ossa unit), (g) Contact between cretaceous limestones and the overlying Eocene–Early Oligocene flysch (Olympos-Ossa unit). The shear bands indicate an ESE-ward sense of movement; shear bands in the blueschists; (h–j) (from Kiliyas [1]) Meso- and microscale structural features and mineral composition of the HP/LT Ampelakia unit in X-Z sections; (h) Shear bands and top-to-SW movement during  $D_2$ , (i)  $S_1/S_2$  fabric, top-to-SW sense of movement, (j) Pyroxene  $\sigma$ -clasts in the intercalated metabasites of the blueschist unit, with glaucophane growing in the pressure shadows of the pyroxenes during the high-pressure process, showing the  $S_1$  fabric.

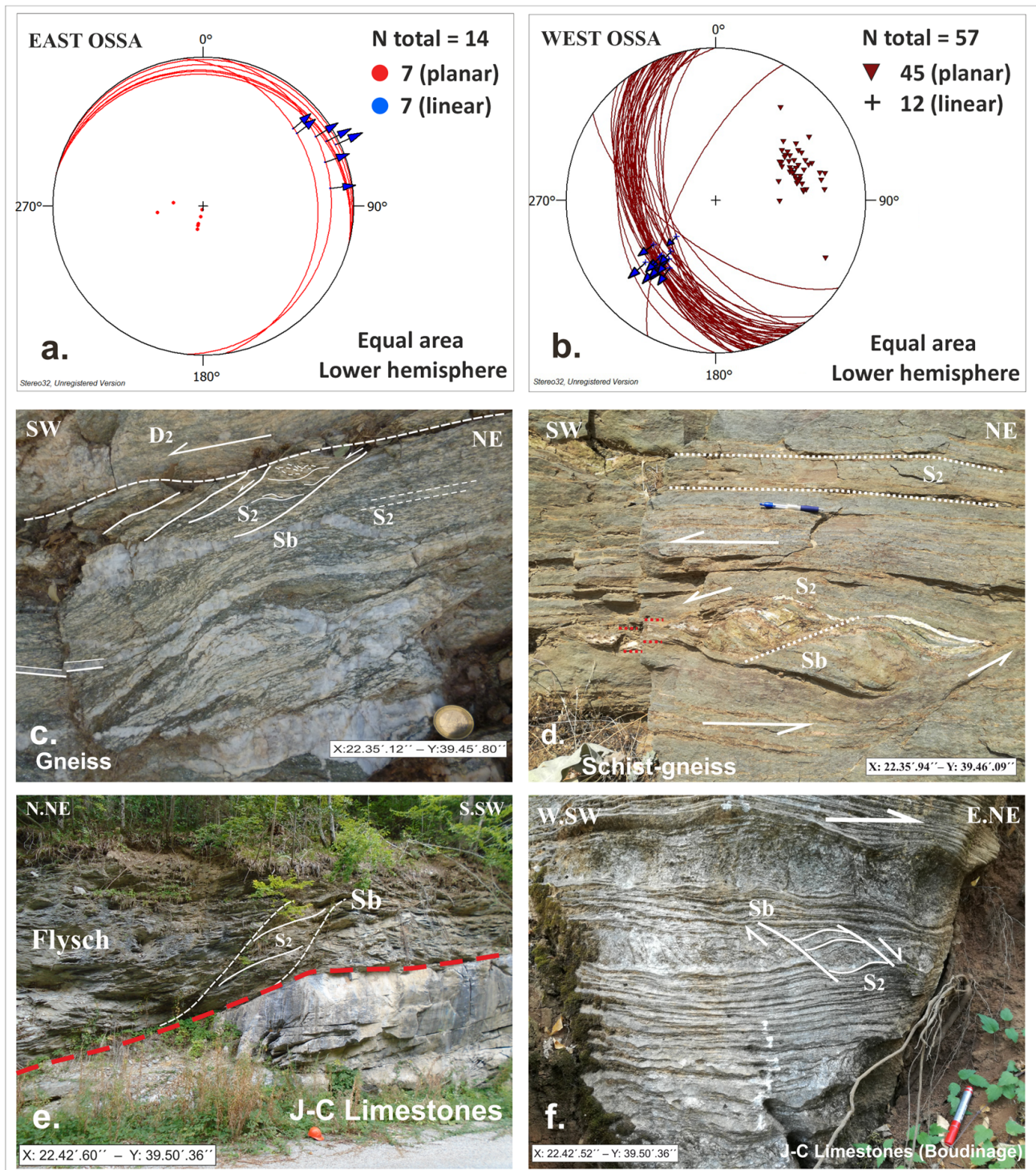


**Figure 4.** (a,b) Schmidt diagrams: Projection of the S<sub>2</sub> foliation and L<sub>2</sub> stretching lineation (equal-area lower hemisphere). The arrows indicate the plunge of stretching lineation; (c–f) Schmidt Macroscale structures and kinematic indicators of the Ossa region: At the western flank: (c) Pelagonian gneiss, (d) Blueschists—Ampelakia unit. The kinematic indicators show a top-to-SW sense of shear. At the eastern flank: (e) Contact between Olympos-Ossa carbonate unit and overlying Eocene flysch (shear bands indicate a NNE-ward sense of movement), (f) Boudinage structures and shear bands show a NE-ward sense of movement.

The D<sub>2</sub> ductile deformation took place under greenschist facies metamorphic conditions, following an isothermal decompression path (Figure 5; [6,8–10,26]). The critical syn-D<sub>2</sub> paragenesis is composed of albite, chlorite, epidote, sericite, actinolite, stilpnomelane, and quartz, which also create the L<sub>2</sub> stretching lineation. Although the glaucophane is recrystallized to actinolite (in places), it is commonly captured in the S<sub>2</sub> planes without any important metamorphic retrogressive indication after its rotation along the S<sub>2</sub> plane. This indicates that the post-D<sub>1</sub>, D<sub>2</sub> deformation took place, at least at its first stages, at a great depth, following the nappe stacking, while the HP rocks' retroward movement was immediate. According to the P-T-t metamorphic path of the blueschist unit (Figure 5), we estimate that this first stage of the D<sub>2</sub> event took place at a depth of ca. 12 km and at a pressure of at least 4 kb, following the last compressional stages of the D<sub>1</sub> and the emplacement of the blueschists on the External Hellenides Olympos-Ossa unit. Furthermore, the extensive dynamic recrystallization of the quartz grains along the S<sub>2</sub> planes, associated with intensive rock mylonitization, indicates an intense ductile D<sub>2</sub> deformation at temperatures exceeding 300 °C [58]. This recrystallization was also performed by grain boundary migration.

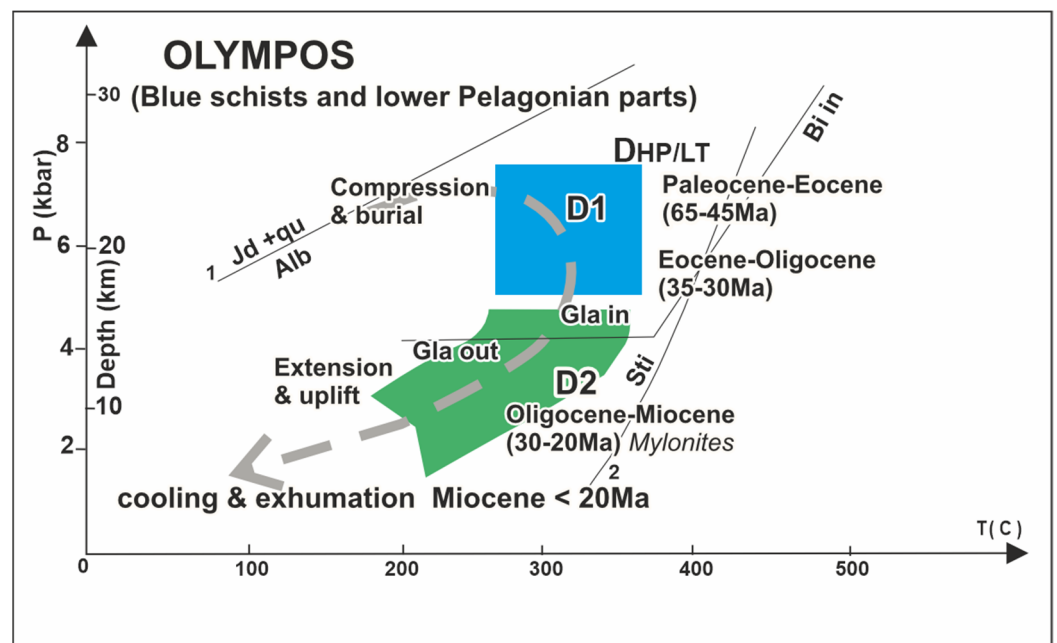


**Figure 5.** P-T-t tectono-metamorphic path and exhumation history of the Paleocene–Eocene high-pressure belt (blueschist) in Olympos-Ossa (modified after [8,10]).

Micro and macro kinematic indicators, such as well-developed S-C structures, shear bands, delta- and sigma-type porphyroclasts, asymmetric boudins, and mica fish (Figures 3, 4, 6–8) reveal, during the D<sub>2</sub> deformation, a main sense of shear down-deep top-to-SW at the western flank and an opposite sense of down-deep top-to-NE at the eastern flank of the Olympos-Ossa region, respectively. This bivergent kinematic geometry highlights a bulk coaxial deformation regime. Furthermore, the quartz C-axis fabric analysis similarly reveals the same geometry of the sense of movement (Figures 9c, 10c, 11c and 12c).

According to the above-described structural data and tectono-metamorphic evolution, the D<sub>2</sub> event should be related to ductile extensional deformation, initiated in a great depth just after the nappe's emplacement, passing further to ductile-brittle deformational conditions. In this case, the D<sub>2</sub> extension was associated with the nappes' tectonic denudation, crustal uplift, and final exhumation of the Ampelakia unit and the Olympos-Ossa unit as a tectonic window. The current tectonic contacts between the several tectonic nappes are considered low-angle, normal detachment faults, previously acting as thrust planes during the nappes stacking.

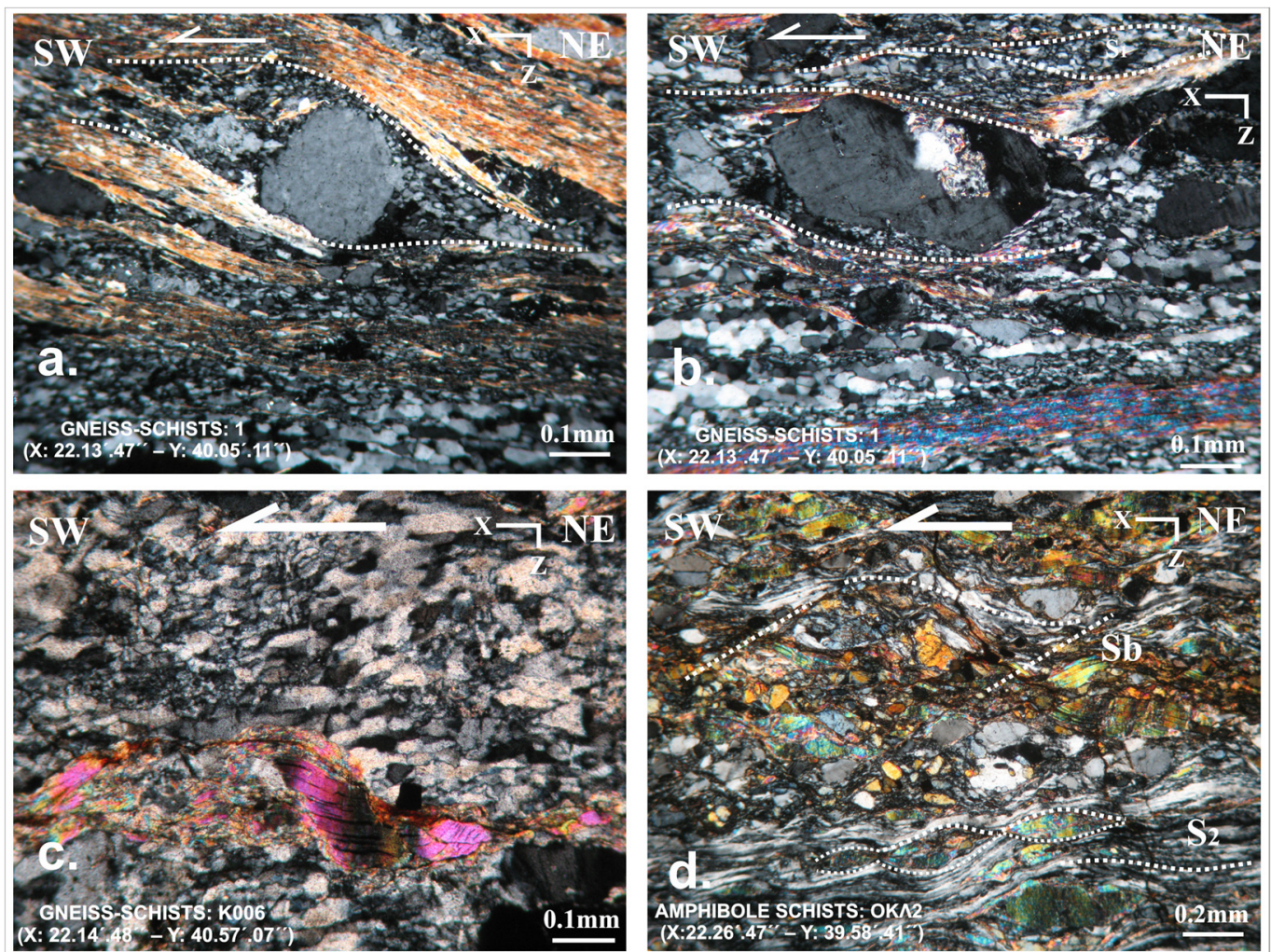


**Figure 6.** Petrographic thin sections, illustrating microscale deformation structures and kinematic indicators in the west (a–c) and south-east (d) Olympus Mountain: (a–c) Feldspar  $\sigma$ -type porphyroclasts, shear bands, and mica-fish, indicating a top-to-WSW sense of shear (Pelagonian schist gneiss); (d) Shear bands and asymmetric boudin structures indicate a WSW-ward sense of movement (Pelagonian amphibole schists).

Considering the described structural and tectono-metamorphic evolution of the Olympus-Ossa mountainous area nappe pile, an Oligocene-Miocene age should be regarded for the D<sub>2</sub> extensional event, as is also described by Schermer et al. [7], Kiliass [10,55], and Kiliass et al. [8,26].

Finally, high-angle normal faults of the Neogene-Quaternary age fragmented all previous structures and geological units. One such high-angle normal fault occurred along the eastern flank of the Olympus-Ossa mountainous area, resulting in significant uplift and the asymmetric geomorphological reconstruction of the Olympus mountain. It is steep at its eastern flank and flat at its western flank.

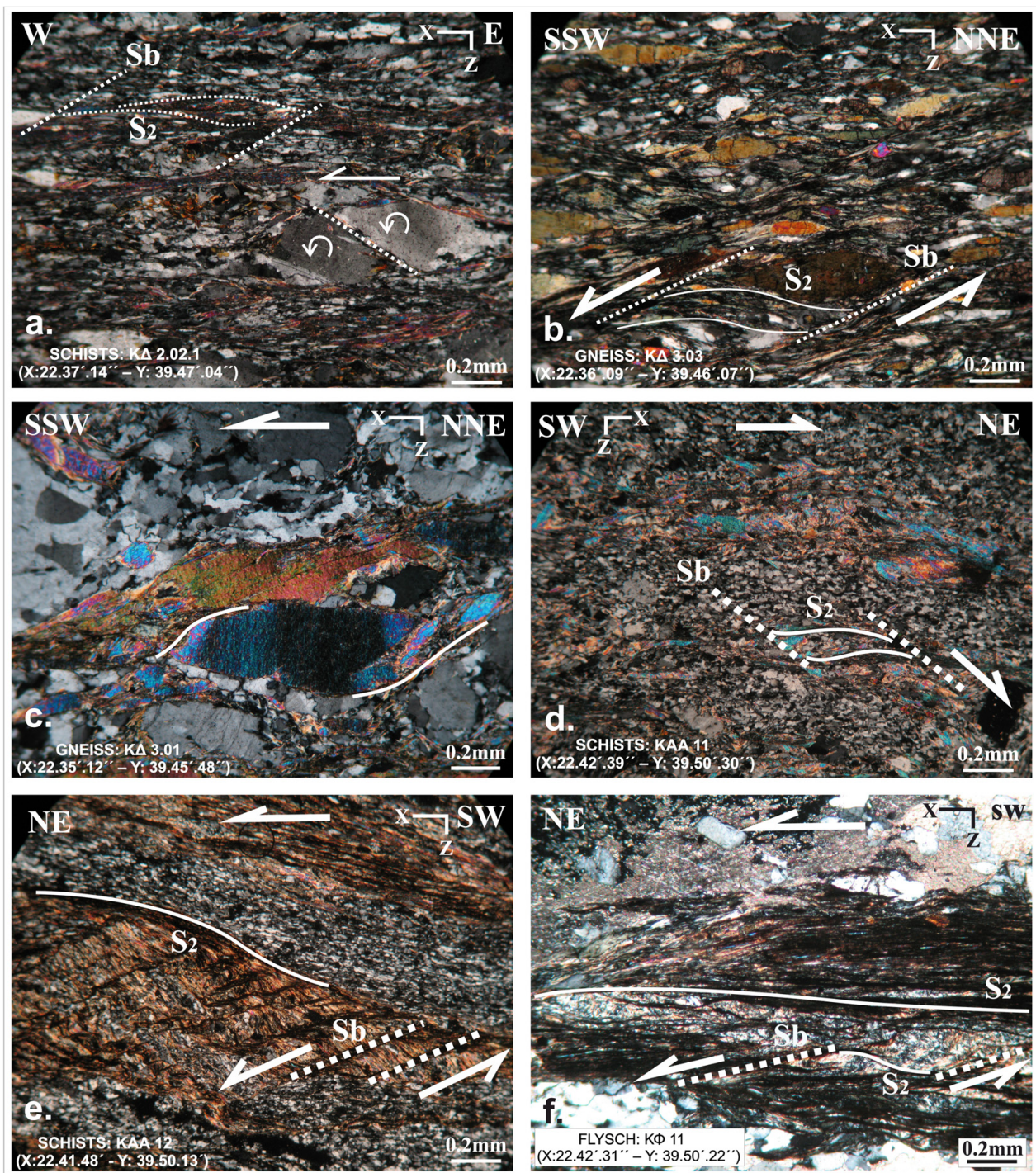


**Figure 7.** Petrographic thin sections, illustrating microscale deformation structures and kinematic indicators in Ossa Mountain. (a–c): Shear bands (Ampelakia schists and Pelagonian gneiss-schists) and mica-fish (Pelagonian gneiss), indicating a top-to-WSW sense of shear at the west flank of Ossa; (d–f): Shear bands (Ampelakia schists and Olympos-Ossa flysch), showing the opposite top-to-NNE sense of shear.

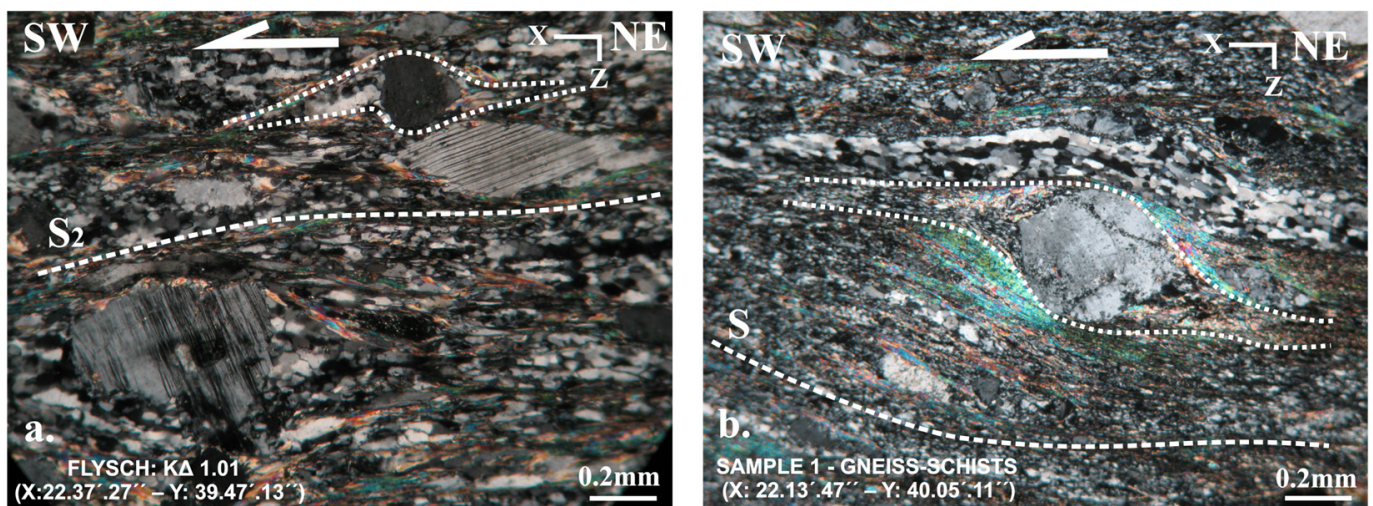


**Figure 8.** Feldspars  $\sigma$ -type porphyroclasts reveal a SW-ward sense of shear. (a) Olympos-Ossa flysch, Ossa Mountain; (b) Pelagonian mylonitic gneiss-schist, Olympos Mountain.

### 3.2. Strain Analysis

#### 3.2.1. Methods

The strain amount of a deformed geological body can be defined by the measurement of the geometric shape of the finite strain ellipsoid, assuming no volume change occurred during the deformational stages [56,57,59].

The ellipticities  $R = X/Z$ ,  $R = Y/Z$ , and  $R = X/Y$  highlight the shape and the quantity of the strain ellipsoid. The finite strain ellipsoid corresponds to the change of shape and (or) volume of an imaginary sphere (with radius equal to unity) due to the several stages of deformation affected by the geological body. The finite strain ellipsoid is characterized by three principal axes, which represent the maximum stretching direction (X-axes), the intermediate stretching direction (Y-axes), and the maximum shortening direction (Z-axes). Three more variables,  $S_X$ ,  $S_Y$ , and  $S_Z$  ( $S_X > S_Y > S_Z$ ), represent the magnitude of the principal strains along these directions. Considering that no volume change occurs, the above three variables are essential to calculate the magnitude of the principal strains and the stretching direction of the ellipsoid.

In our qualitative and quantitative analysis investigation, 18 oriented samples were collected along the C and D cross-sections of Ossa Mountain (Figures 9a,b and 10a,b), while 15 oriented samples were collected along the A, B1, and B2 cross-sections of Olympos Mountain, respectively (Figures 11a,b and 12a,b,d). For calculating the finite strain ellipsoid, each sample was prepared in at least two thin sections, the first one parallel to the  $L_2$  stretching lineation, and the other vertical, both to the  $L_2$  lineation and the  $S_2$  foliation. Feldspars and quartz grains were implemented in the calculations. The Rf/ $\phi$ , Fry, and Panozzo methods [56,60,61] were applied to 66 thin sections running the “fabric 8” software [62]. The aspect ratios and the three-dimensional strain geometry were calculated by implementing the mathematical equations shown in (Figure 13). Finally, all measurements are projected in the Flinn [63] and Nadai [64] diagrams in order to determine the shape of the finite strain ellipsoid and the type and intensity of deformation.

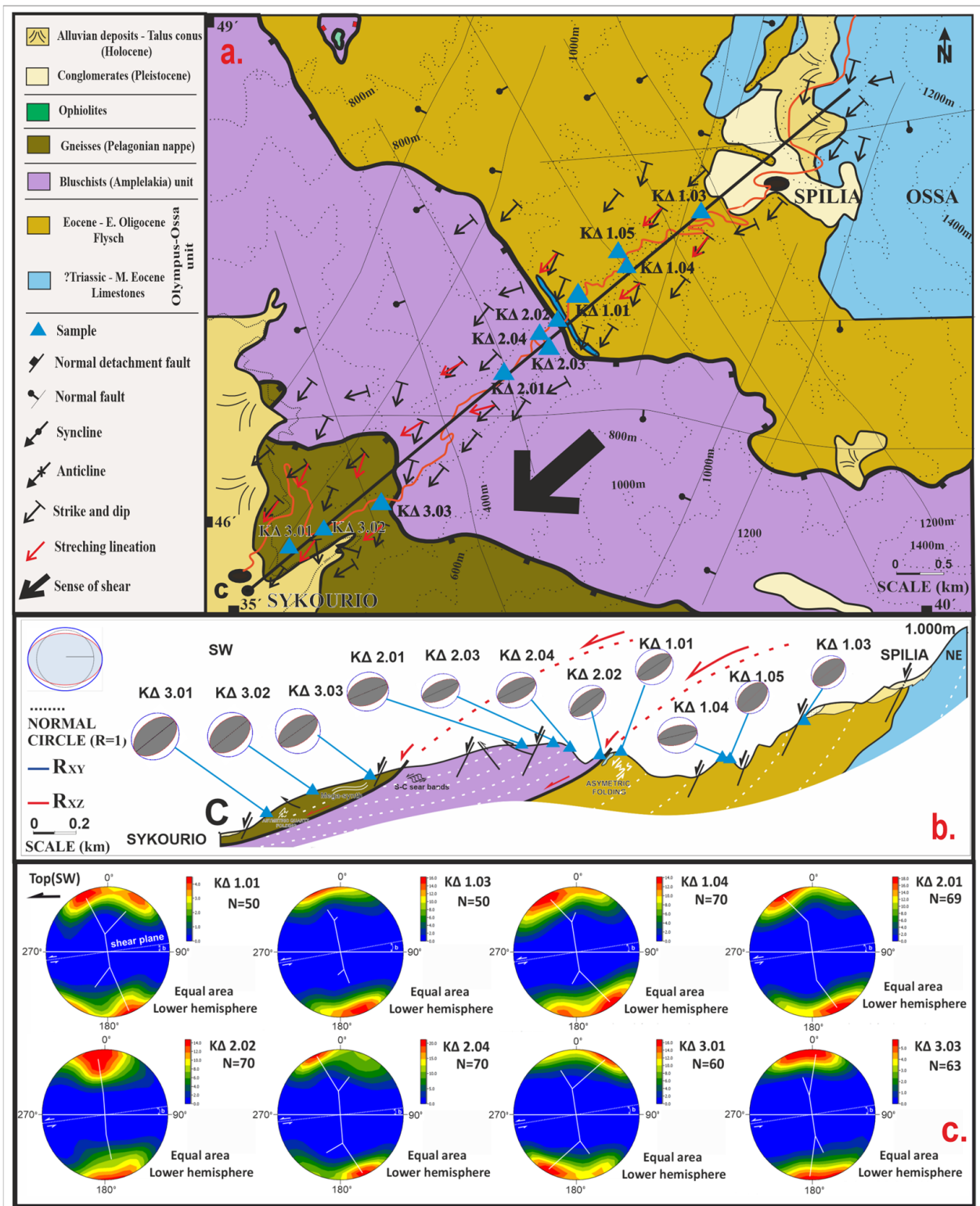


**Figure 9.** (a) Geological map of the west Ossa area (modified after [65]); (b) Cross-section C and the calculated strain ellipsoids across the section are shown; (c) Quartz C-axes diagrams showing the sense of movement and a flattening type of deformation, drawn using the “Stereo 32” software [66,67].

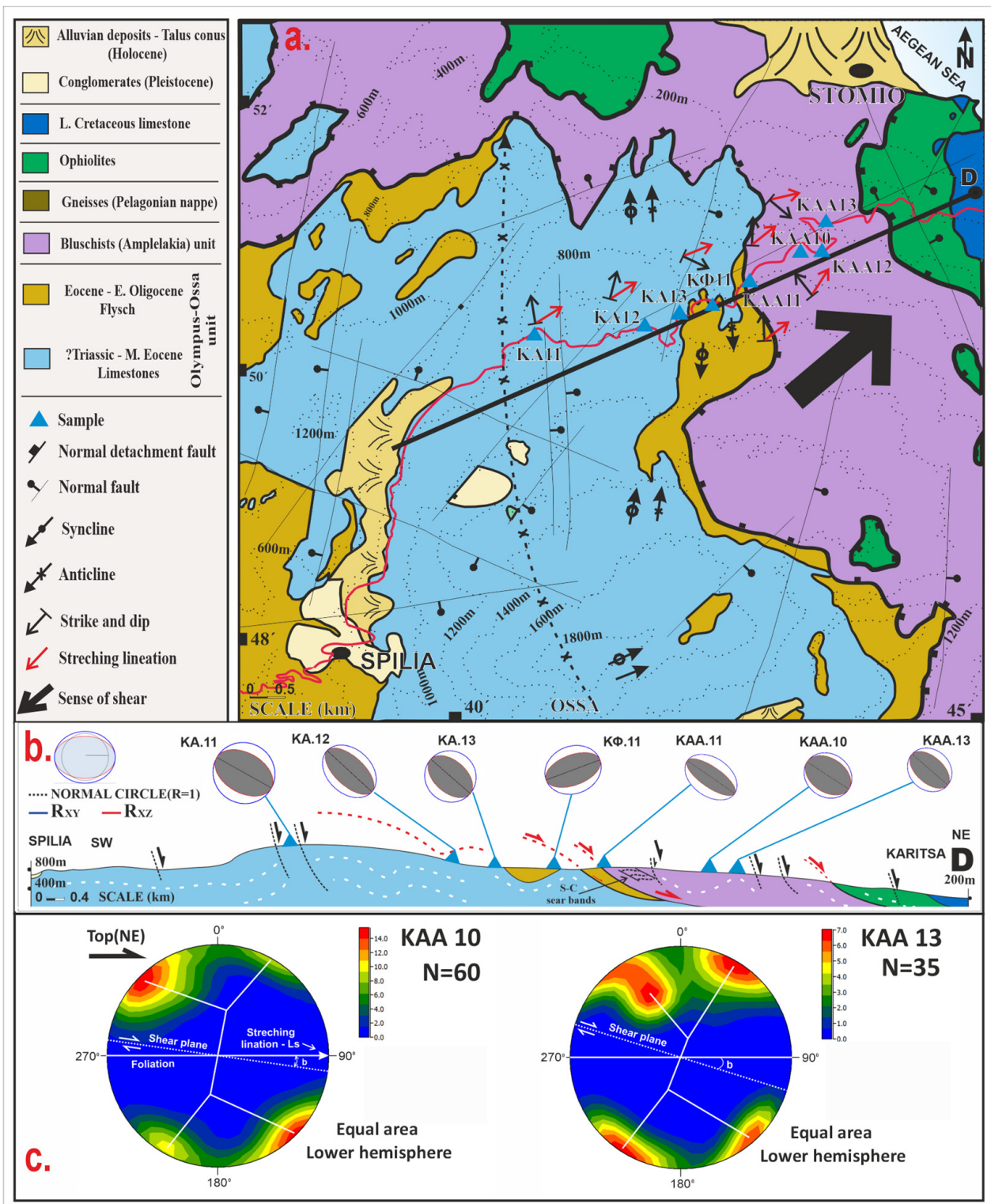


**Figure 10.** (a) Geological map of the east Ossa area (modified after [65]); (b) Cross-section D and the calculated strain ellipsoids across the section are shown; (c) Quartz C-axes diagrams showing the sense of movement and a flattening type of deformation, drawn using the “Stereo 32” software [66,67].

**Rf/phi method [68,69]:** This method is based on the measurements of the long and the short ellipsoid axes on both the XZ and YZ planes. The method considers homogenous deformation in the view scale, as well as that the grains are elliptical and distributed randomly. The exporting data show the final ellipticity (Rf) and the phi ( $\phi$ ) angle between

the long X-axes and the foliation, e.g., (Figure 14a). The  $X^2$ -test diagram verifies these results of Rf/phi magnitude.

Fry method [56,60,70,71]: This method is generally based on the relative displacement of several porphyroclasts. (e.g., feldspars, quartz grains, hornblende, and mica). In this study, the central points of quartz grains in the thin sections were analyzed by the normalized Fry method, applying the “fabric 8” software [62], and then the center point of grains forms an ellipse, which determines the final orientation and the long and short axis of the finite strain ellipse. The requirements for this method are the same as those described for the Rf/phi method above. A graphic example of the extracted results is shown in (Figure 14b), including the final ellipsoid ( $R, \phi$ ) in the matrix of the grain center and the verification of the final ellipticity diagram (d-a).

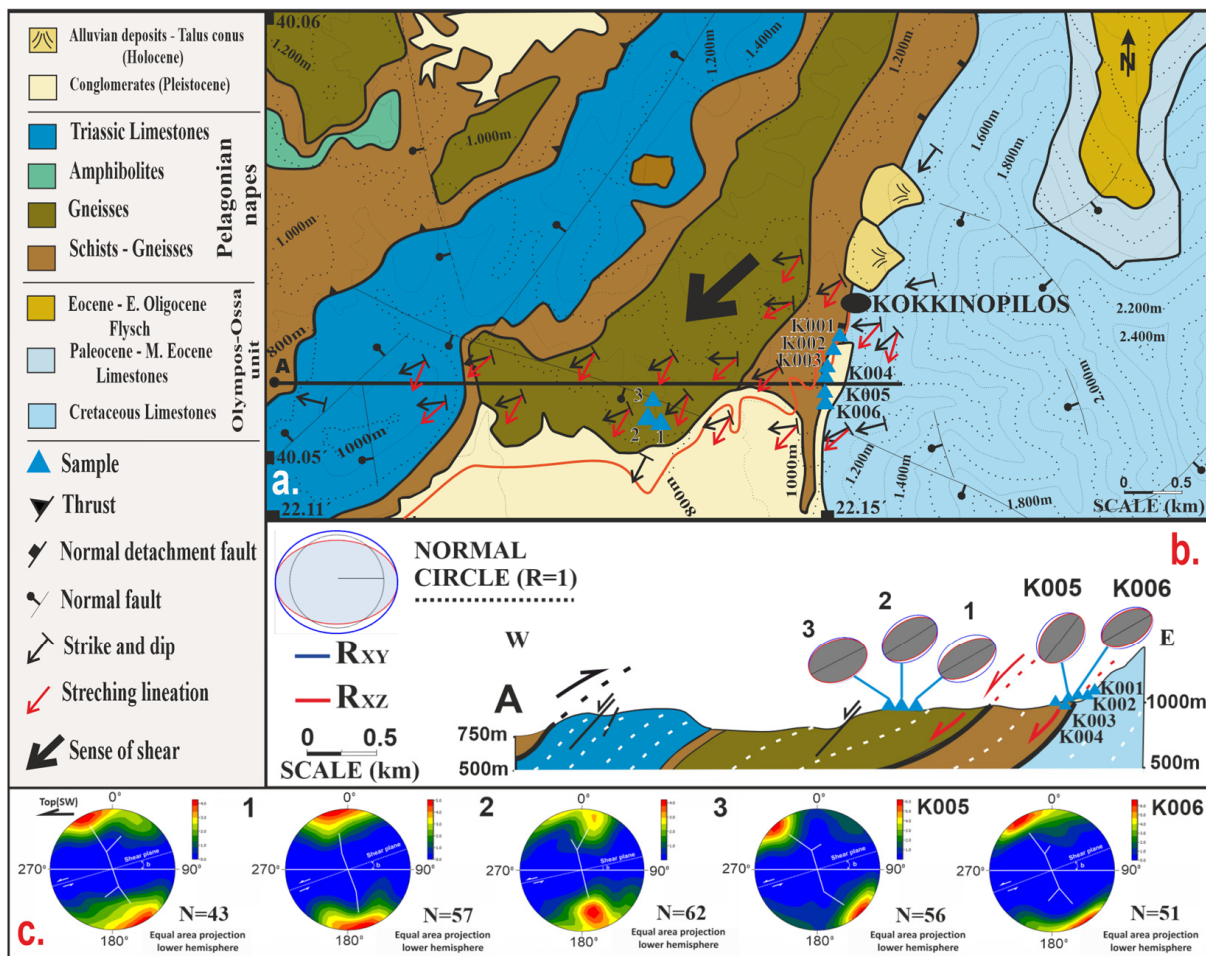


**Figure 11.** (a) Geological map of the west Olympos area (modified after [72]); (b) Cross-section A and the calculated strain ellipsoids across the section are shown; (c) Quartz C-axes diagrams showing the sense of movement and a flattening type of deformation, drawn using the “Stereo 32” software [66,67].

Panozzo method [61,73]: This method is applied for computing the two-dimensional strain ellipse. The outlines of grains’ shapes are digitized as closed polygons and then projected onto a reference line. An example of our results is depicted in (Figure 14c).

Furthermore, to determine the deformation type and sense of movement, quartz C-axis diagrams were constructed, measuring the quartz C-axes orientation in (8) eight X-Z thin-sections of the Olympos area units and (10) ten X-Z thin-sections of the Ossa area units, using the Fedorow table methods [58,74]. The C-axes orientation data, using the “Stereo 32” software,

Version: 1.0.1 [66,67], were projected in Schmidt stereograms (lower hemisphere, equal area) for the construction of the corresponding C-axis diagrams (Figures 9c, 10c, 11c and 12c).

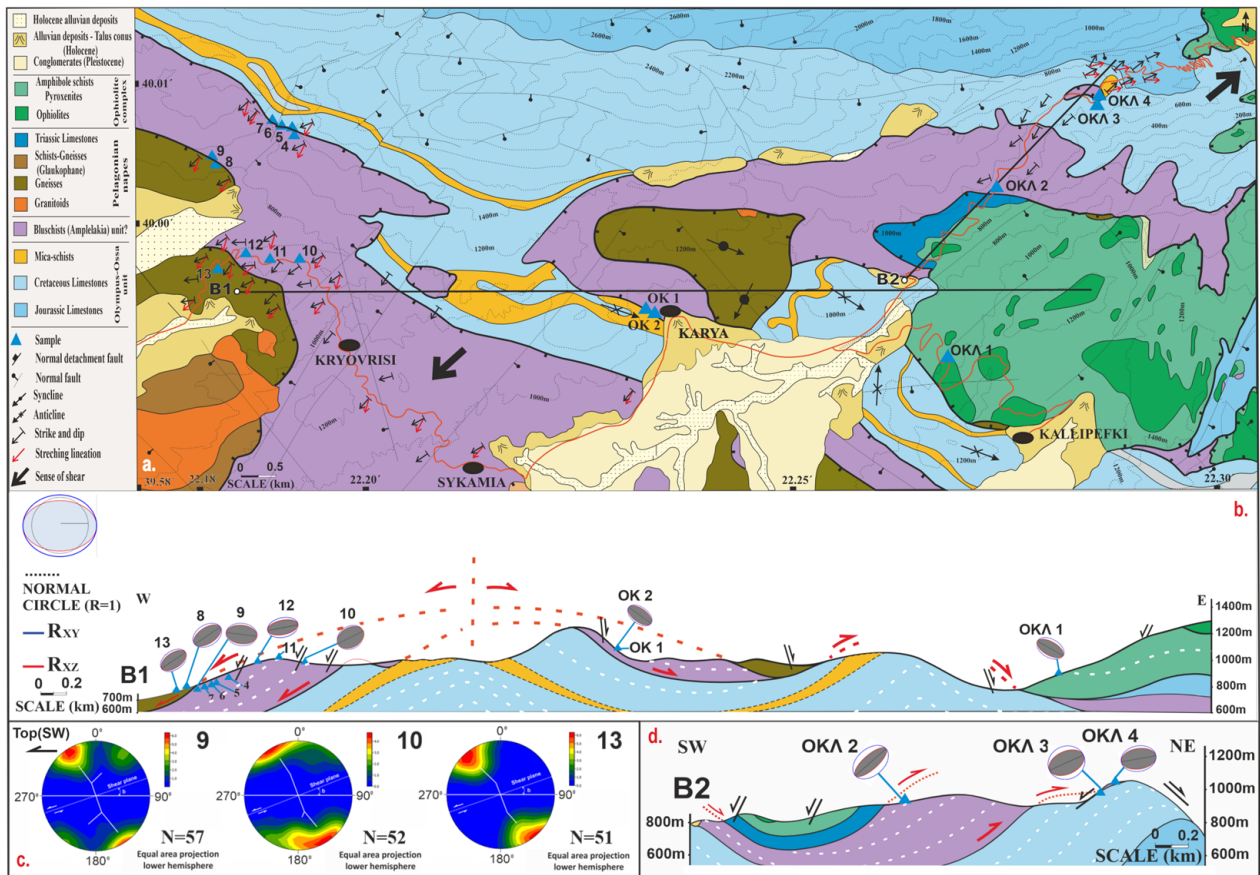


**Figure 12.** (a) Geological map of southwest Olympus area (modified after [75]); (b,d) Cross-sections of B1 and B2 and the calculated strain ellipsoids are shown across the sections (B1, B2); (c) Quartz C-axes diagrams showing the sense of movement and a flattening type of deformation, drawn using the “Stereo 32” software [66,67].

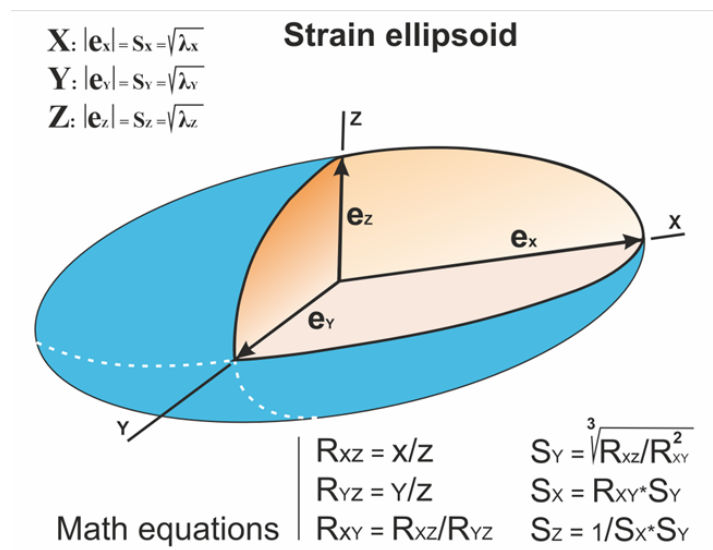


**Figure 13.** Geometry and math equations of the strain ellipsoid, which is characterized by the three main strain axes  $X > Y > Z$ .  $e_x$ ,  $e_y$ , and  $e_z$ : the strain intensity along the main strain axes.

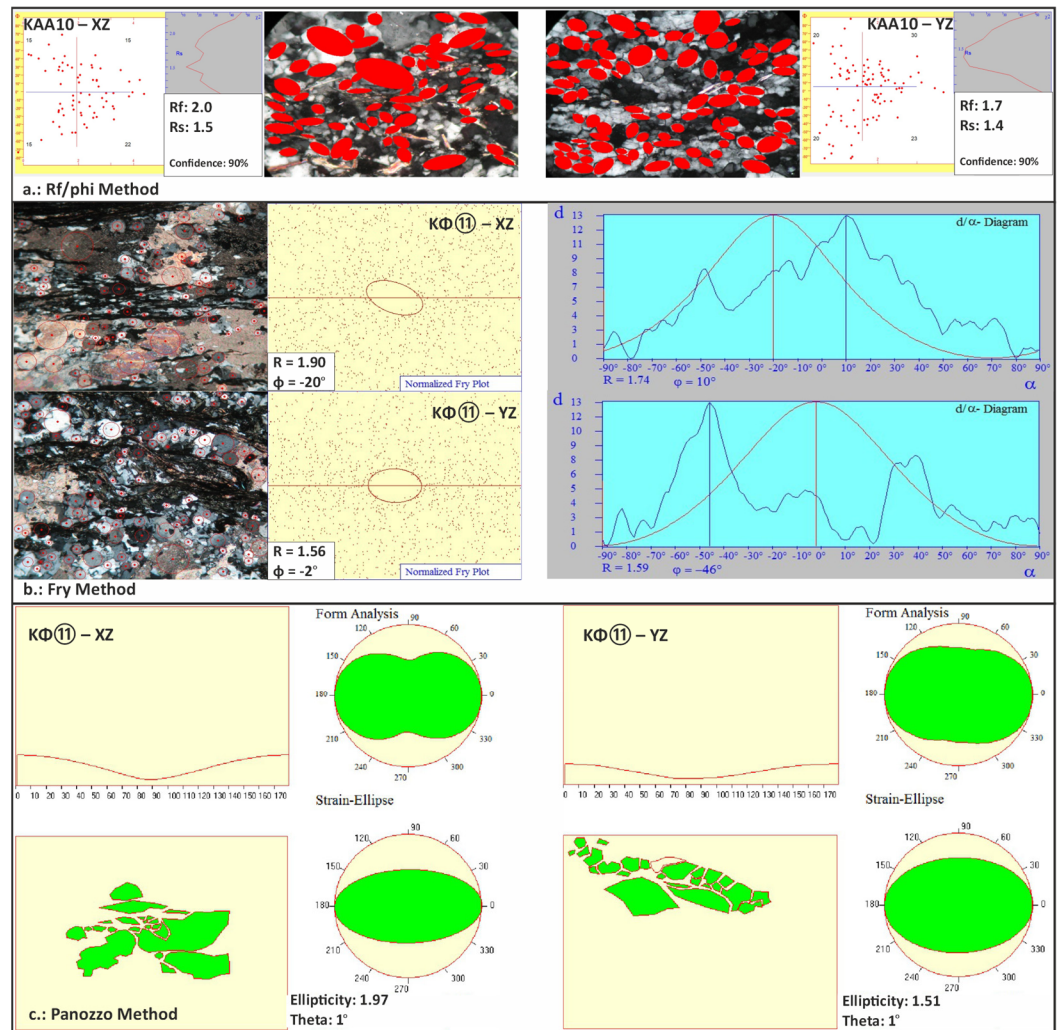


**Figure 14.** The Rf/phi (a), Fry (b), and Panozzo (c) methods calculated finite strain ellipses in the XZ and YZ deformation planes, applying the “fabric 8” software [62].

The vorticity number  $W_k$  [57,58]. There are many used methods for estimating the kinematic vorticity number  $W_k$ . In this study, we focused on 2D flows, in which the plane of observation is parallel to the XZ section plane of the sample. The vorticity number  $W_k$  was calculated to define the component of the non-coaxial rotation in the plastic flow. In particular, the simplified mathematical formula, which is based on the original formula by Wallis [76,77], and modified by Xypolias [78], was implemented:  $W_k = \cos^*\{\tan^{-1} * [(1 - R_{xz} * \tan b^{-2}) / (1 + R_{xz}) * \tan b]\}$ .

This technique considers the calculation of the strain ratio  $R_{xz}$  and the  $b$  angle between the shear/flow plane and the main foliation. The shear plane and foliation are drawn in C-axis diagrams. The perpendicular line to the central arm of the quartz C-axis diagram should be drawn to find the shear/flow plane. In our quartz C-axis diagrams, due to the flattening type of the deformation, the central arm was designed based on the calculated skeleton asymmetry, while the  $W_k$  values were approximately calculated (Tables S1–S6).

The actual shape of the ellipsoid is determined by the parameter  $k = (R_{XY} - 1) / (R_{YZ} - 1)$ , where  $R_{XY}$ ,  $R_{YZ}$  is the ratios of the principal strain axes X, Y, Z of the ellipsoid. The  $k$  parameter values are represented in the Flinn diagram [63]. Accordingly, the Nadai diagram illustrates the Lode parameter, which provides the strain type in a similar way to the Flinn diagram, based on the distance from the origin of the axes, which illustrates the total strain magnitude [64].

### 3.2.2. Strain Data

Based on our measurements and fabric analysis, it seems that the strain intensity generally increases from the Olympos-Ossa unit to the Pelagonian nappe, excepting some individual values, usually along the nappe contacts. The values of these measurements are analytically shown in Tables S1–S6. In the Ossa region, the measured strain values range: for  $S_x$ , from 1.039 to 1.784, for  $S_y$ , from 0.993 to 1.323, showing extension in the Y direction ( $Y > 1$ ), and for  $S_z$ , from 0.505 to 0.982. Accordingly, in the Olympos region, the measured strain values range: for  $S_x$ , from 1.168 to 1.812, for  $S_y$ , from 0.931 to 1.241, showing extension in the Y direction ( $Y > 1$ ), and for  $S_z$ , from 0.490 to 0.852 (Tables S1–S6; Figures 9–12). These ranges of magnitudes indicate no significant differences in the strain values between both Olympos and Ossa mountainous areas but increase systematically along the tectonic contact between the several tectonic nappes (Figures 9–12). Furthermore, the projection of the finite strain data in the Flinn and Nadai diagrams (Figures 15 and 16) show that both the western and eastern Olympos-Ossa mountainous flanks are characterized by a main flattening type of the strain ellipsoid ( $Y > 1$ ), while limited deviations to near plain strain ( $Y = 1$ ) are also documented.

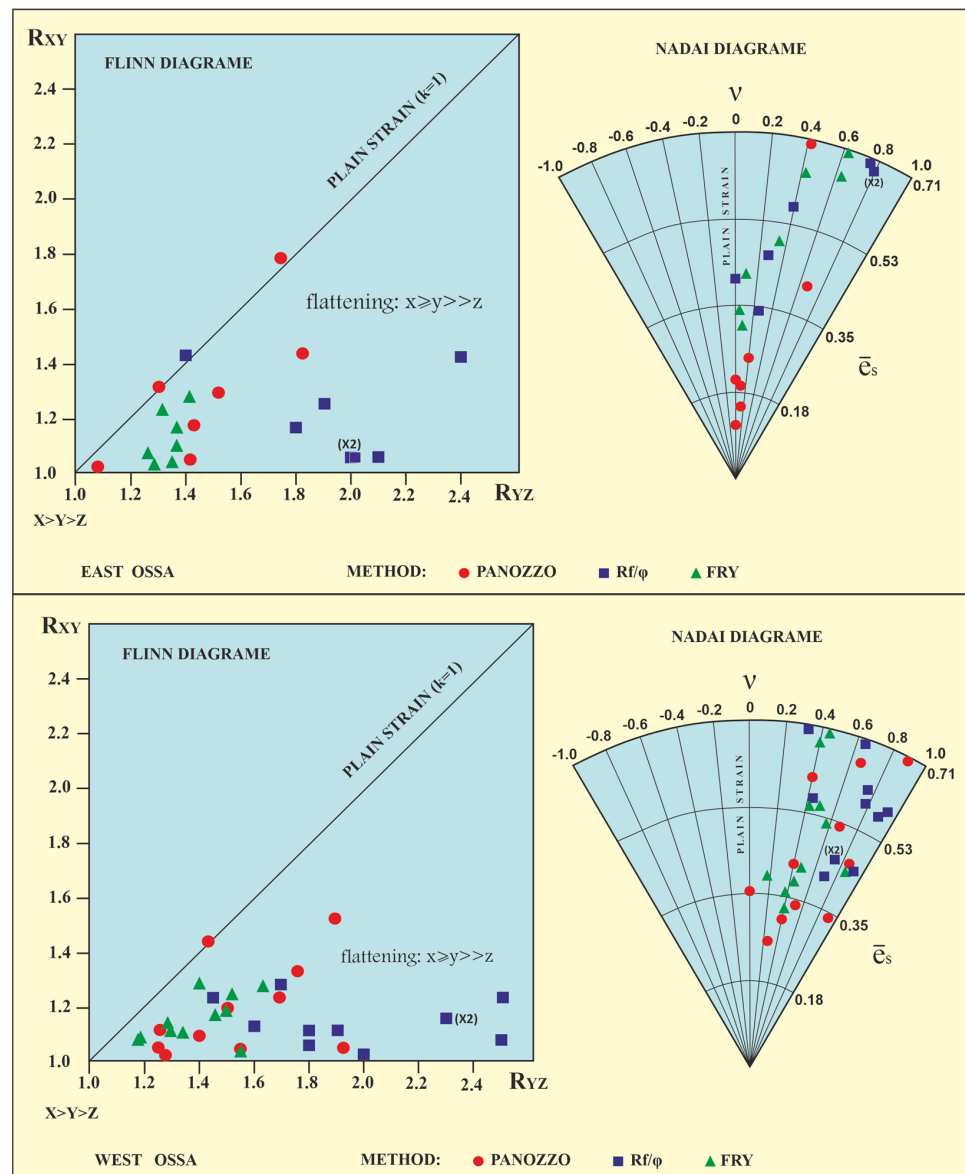


**Figure 15.** Strain analysis results in the area of Mount Ossa, plotted onto Flinn and Nadai diagrams  $K = (R_{xy} - 1)/(R_{yz} - 1)$ , applying the “fabric 8” software [62].

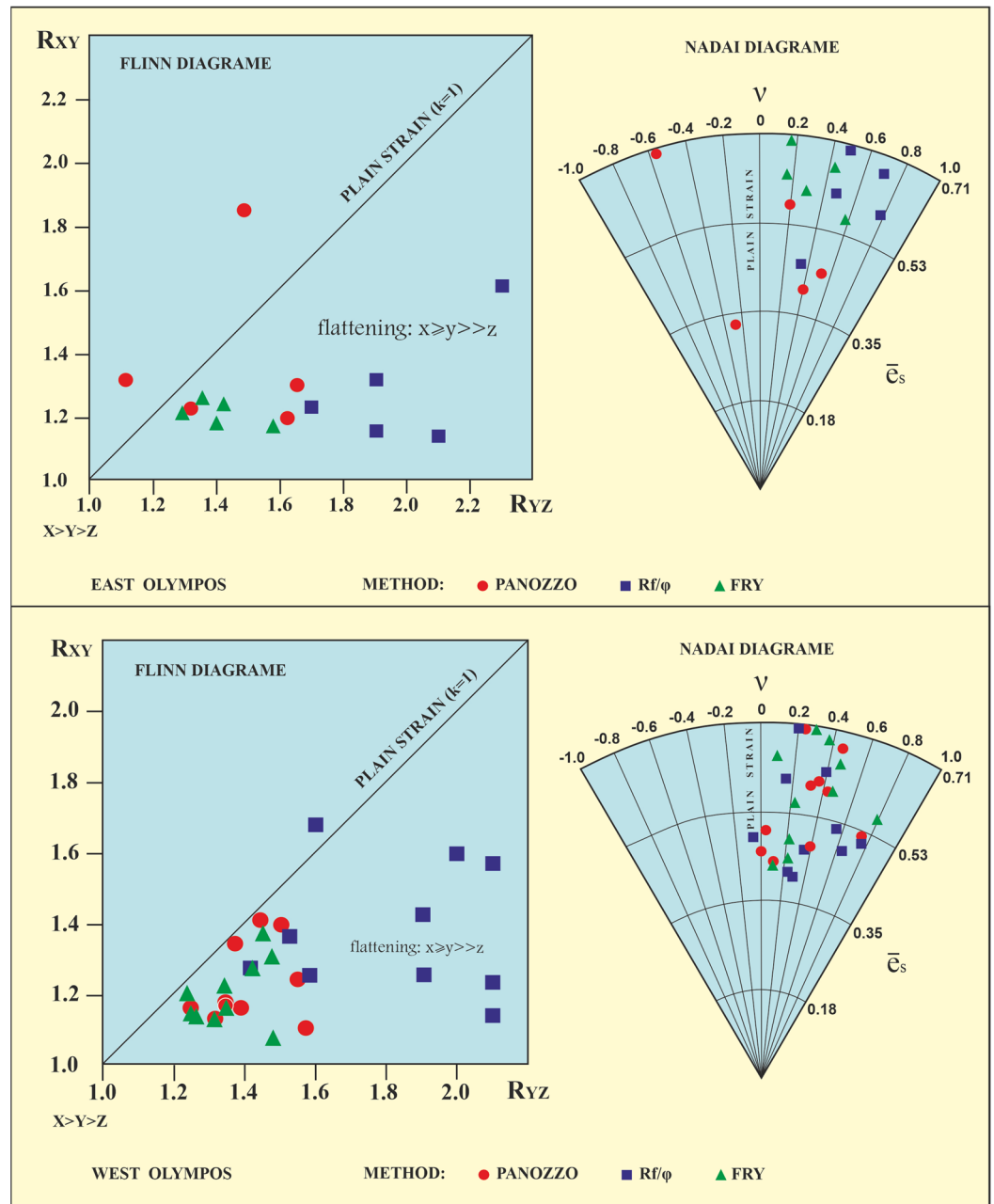


**Figure 16.** Strain analysis results in the area of Mount Olympos, plotted onto Flinn and Nadai diagrams,  $K = (R_{xy} - 1)/(R_{yz} - 1)$ , applying the “fabric 8” software [62].

The resulting quartz C-axes diagrams form a skeleton by small circle girdles, while no central branch of fabric occurs, indicating a flattening type of deformation (Figures 9c, 10c, 11c and 12c). These diagrams highlight approximatively the shear plane because the central band section is not clearly recorded but the direction of movement is very well indicated by the asymmetry of the small circle girdles: The direction of movement is constantly W-SW-ward at the west flank and E-NE-ward at the east flank of the Olympos-Ossa mountainous region, respectively (Figures 9–12). Furthermore, the developed asymmetric skeletons, with a predominant and a secondary one, reflect a non-coaxial flow and a simple shear component [79–83].

The calculated  $W_k$  values of the Olympos region range from 0.23 to 0.78, while the corresponding  $W_k$  values of the Ossa region range from 0.52 to 0.93 (Tables S1–S6). As shown in (Figure 17a–c), the simple shear component shows a gradual increase from the

deeper tectonic units (Olympos-Ossa unit) to the upper Pelagonian nappe, and the  $W_k$  values of the Ossa region record higher values than the Olympos ones. Nevertheless, great values of  $W_k$  were generally recorded within the Ampelakia unit, indicating an important simple shear component in this unit, which is recorded as the suture zone between the carbonate Olympos-Ossa unit (External Hellenides) and the Pelagonian nappe pile (Internal Hellenides). Furthermore, the range of the  $W_k$  value of our study area [78] is compared to the Hellenides (Figure 17d). This diagram shows that the estimate of  $W_k$  values of the Olympos-Ossa area and the Hellenides are in good agreement.

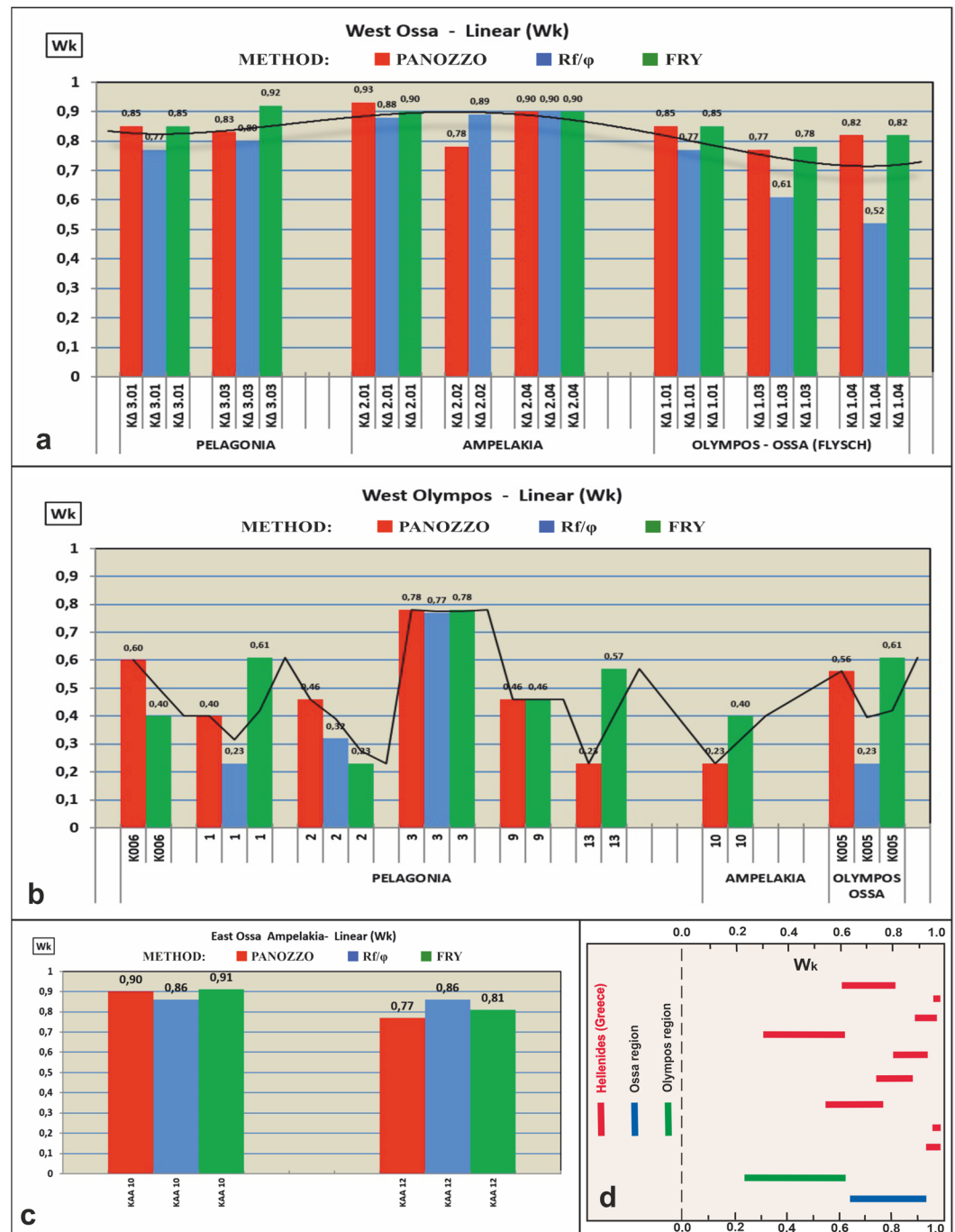


**Figure 17.** The linear change of  $W_k$  values. (a): W. Ossa; (b): W. Olympos region; (c): E. Ossa and (d): Hellenides. The range of  $W_k$  values in the Olympos-Ossa area, compared to the  $W_k$  value ranges of the Hellenides. (modified after [78]).

The strain analysis with which the deformation is quantified highlights, generally, the finite strain. Finite strain represents the accumulation of the overall ductile strains affected by a structural unit. In our case, through the different deformational stages recognized in the studied structural units, the dominant ductile event is clearly the last  $D_2$  one. Pre- $D_2$  strains were overprinted or obliterated by  $D_2$ , as indicated by the pre- $D_2$  relict structures. Therefore, it is assumed that the calculated finite strain measurements are strongly controlled by the  $D_2$  and represent the accumulation of the pre- $D_2$  and  $D_2$  strains, while the pre- $D_2$  strains accumulated in the studied tectonic units cannot be separated. The resulting finite strain geometry with local variations in geometry is interpreted as the result of heterogeneous deformation during the dominating  $D_2$  event.

#### 4. Discussion

As has already been mentioned, many researchers have studied the Olympos-Ossa mountainous region. However, no clear interpretation considering the geotectonic evolution of this area has been provided, while some queries remain under discussion.

Lips et al. [3] applied the  $^{40}\text{Ar}/^{39}\text{Ar}$  laser probe age-dating technical method, concluding that a top-to-NE direction of tectonic emplacement of the HP Ampelakia unit and the Pelagonian nappe on the Olympos-Ossa unit took place at the time interval between the ca. 85–54 Ma. Subsequently, at ca. 54 Ma, a shift in the dominant direction of nappes tectonic denudation from NE-ward to WSW-ward is documented, related to the blueschist exhumation and crustal thinning.

Furthermore, kinematic evidence for ENE-ward tectonic emplacement of the blueschist and the Pelagonian nappe on the Olympos-Ossa carbonate unit during Paleocene–Oligocene was concluded by Xypolias et al. [13] and Gerogiannis & Xypolias [25] for the Cyclades and Pelion study area. The same NE-ward kinematic direction for these Paleocene–Oligocene nappes stacking in the Olympos area was also proposed by Nance [54]. The NE-ward emplacement direction of the nappes pile is opposed to the observations by Kiliass [10,55], Kiliass et al. [8], and Schermer [9], who conclude SW-ward tectonic emplacement of the HP/LT Ampelakia unit and the Pelagonian nappe on the Olympos-Ossa unit during the Eocene–Early Oligocene. Subsequently, Oligocene–Early Miocene ductile extension caused the final exhumation of the HP/LT Ampelakia unit and the Olympos-Ossa carbonate unit as a tectonic window. Moreover, according to several authors, e.g., Wernicke [84], Dewey [85], Gautier & Brun [86], Ring & Glodny [15], and Lister & Forster [19], the syn-orogenic extension is the key to the exhumation mechanism of HP rocks.

Moreover, according to Ring et al. [11,12], Ring & Glodny [15], and Xypolias et al. [22], the early stage of the retoward and exhumation of HP rocks is related to an extrusion wedge process. This extrusion wedge is bounded at the top by a normal detachment fault and at the base by a thrust fault or an out-of-sequence thrust fault, without requiring a lithospheric extension. Both thrust and normal faults act simultaneously. The thrusting of the HP rocks in Evia Island initiated their motion during the Early Eocene after their burial in ca. 20–25 Km in-depth and metamorphism under HP/LT conditions, while it was completed with their emplacement onto the carbonate Almyropotamos basal unit, regarded as equivalent to the Olympos-Ossa unit [1], during the Late Eocene–Oligocene [15].

According to our study, two main stages of deformation were recognized in the Olympos-Ossa mountainous area. The first  $D_1$  stage was associated with compression, nappes stacking, blueschist facies conditions, and the final SW-ward tectonic emplacement of the HP/LT Ampelakia unit and the Pelagonian nappe pile on the Olympos-Ossa unit during the Paleocene–Early Oligocene. The second stage of the  $D_2$  deformation is related to retrograde greenschist facies metamorphism of the Oligocene–Miocene age, crustal uplift, and final exhumation of the Olympos-Ossa unit under bivergent SW-ward and NE-ward extension, initially ductile and subsequently ductile to brittle. An extrusion wedge process for the HP/LT rocks should be the main mechanism for their earlier exhumation and tectonic emplacement. Nevertheless, in our study area, we have not observed the main basal thrust fault and the extensional shear zone related to the lateral extrusion wedge of

the HP/LT Ampelakia unit during its early exhumation stages, as it was described by Ring and Glodny [15] for the Evia and Cyclades areas. The observed tectonic contact between the lowermost Olympos-Ossa unit and the HP/LT Ampelakia unit was interpreted as a normal detachment fault, while the other main tectonic contact between the Ampelakia unit and the uppermost Pelagonian nappe was also recognized as a normal detachment fault. We interpret the absence of the main basal thrust fault, along which the HP/LT rocks were emplaced initially onto the Olympos-Ossa unit, as well as the absence of the simultaneous main normal detachment at the top of the HP/LT rocks, due to the intense overprint of the younger D<sub>2</sub> Oligocene–Miocene extensional regime. We suggest, in agreement with Kiliias [1,10,55] and Kiliias et al. [8,26], that the final exhumation of the Ampelakia blueschist and Olympos-Ossa units was performed due to the occurrence of this second ductile and progressively brittle-ductile D<sub>2</sub> event, as it is clearly indicated by the description of its structural and metamorphic setting. It is summarized in the development of the opposite SW- and NE-ward downwardly moved structural units, related to flattening type ductile deformation, at both SW- and NE-flanks of the Olympos-Ossa mountainous area, respectively. This structural geometry, associated with retrograde decompressional metamorphism, caused the bivergent tectonic nappes denudation, crustal uplift, and final exhumation of the Olympos-Ossa tectonic window (Figure 18). In addition, the Eocene–Early Oligocene emplacement of the Paleocene–Eocene HP/LT Ampelakia unit and the Pelagonian nappes pile on the Olympos-Ossa unit are associated with a lateral extrusion wedge under compressional tectonic, following the Ring et al. [11,12], Ring & Glodny [15], and Xypolias et al. [22] models, and further through an out-of-sequence thrusting, resulting in the final emplacement of the Pelagonian nappe pile on both the HP/LT rocks and the Olympos-Ossa unit.

A dynamic unstable overthickening crust due to nappes stacking processes could well explain the transformation of compression (D<sub>1</sub>) to extension (D<sub>2</sub>), further related to the orogenic collapse. Tertiary retreating and rollback of the subducted Pindos-Cyclades lithospheric slab under the Pelagonian nappe, as described by Ring et al. [12,27] and Kiliias [1], could also be the mechanism for the change of the dynamic status in the Hellenic orogenic system of compression to extension. The Neogene-Quaternary high-angle normal faults and the great normal fault bounded the eastern high-angle dipping flank of the Olympos-Ossa mountainous area, progressively following the D<sub>2</sub> extension, forming the final geomorphological relief of the Olympos-Ossa Mountain (Figure 18).

Considering the strain analysis data and results the recorded difference in  $W_k$  values in the Olympos and Ossa regions, which are greater in Ossa than Olympos, possibly highlights a difference in timing of the whole exhumation process in the two regions, respectively. Moreover, the high  $W_k$  values calculated within the HP-LT Ampelakia unit notes the tectonic contact between the External Hellenides Olympos-Ossa unit and the Internal Hellenides Pelagonian nappes pile as an important suture zone. Additionally, strain intensity near or along the nappe tectonic contacts supports the described nappes pile structure of the study Olympos-Ossa area and its evolution. On the other hand, the quartz C-axes diagrams indicate a significant component of a non-coaxial deformation, flattening type of deformation, and sense of shear similar to the described direction of movement, inferred in the field and in the microscope using kinematic indicators data. In this case, it is concluded that finite strain analysis, micro-fabric analysis, and vorticity number calculations all support the proposed deformation history.

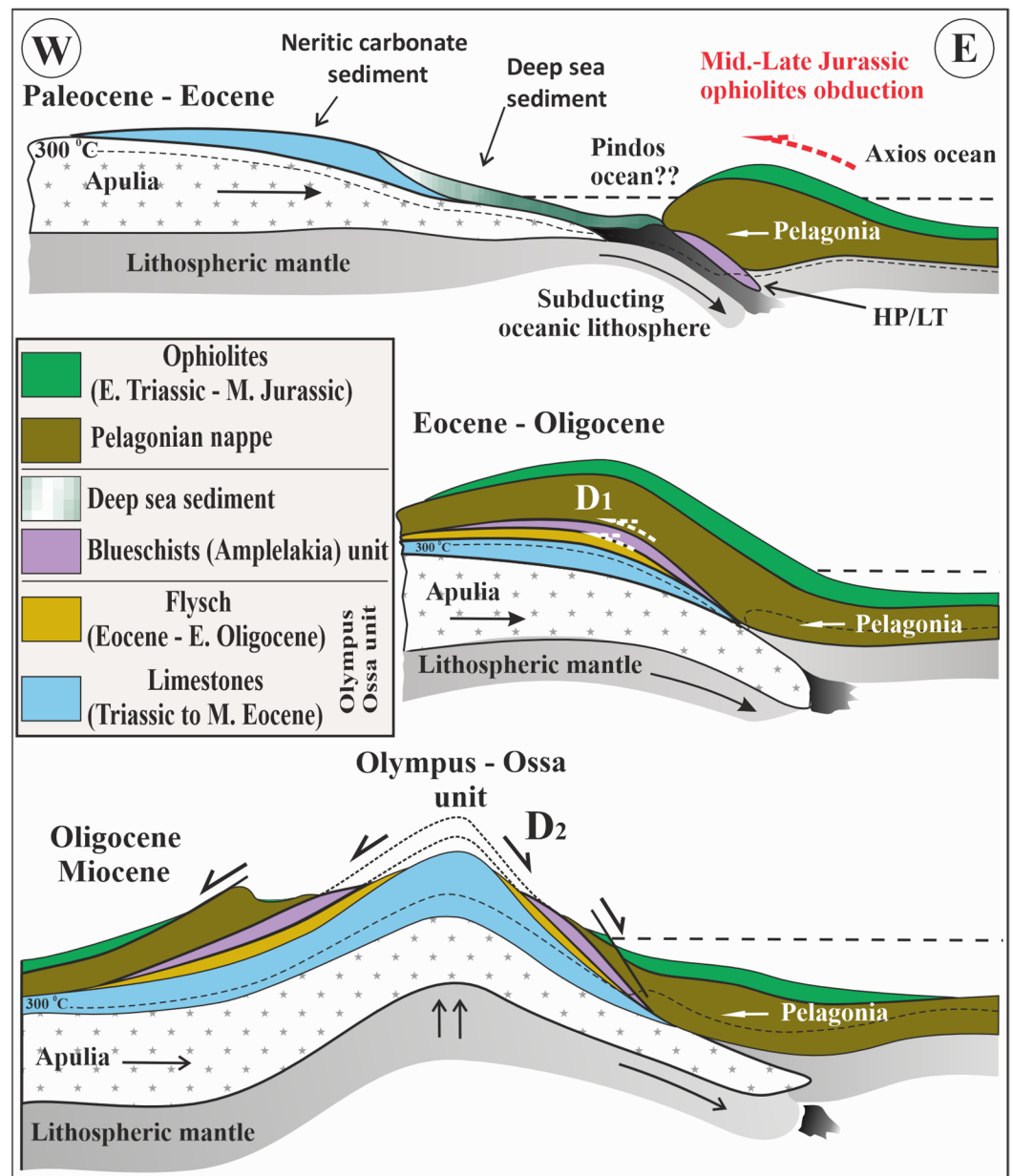


**Figure 18.** Schematic crustal-scale transects showing, stepwise, the paleo-geographic and geotectonic evolution of the Olympus-Ossa mountainous area. Paleocene-Eocene subduction, HP/LT metamorphism, and nappes stacking during compressional tectonics. Eocene–Early Oligocene emplacement of the Pelagonian nappe and the blueschists of the Olympus-Ossa unit. Oligocene–Miocene extension and final exhumation of the HP/LT Ampelakia unit and the External Hellenides Olympus-Ossa carbonate unit.

**5. Conclusions**

Conclusions from the finite strain and structural fabric study of the HP/LT Ampelakia unit and carbonate Olympus-Ossa tectonic window exhumation process are as follows:

1. The HP/LT metamorphosed Ampelakia unit during the Paleocene–Eocene subduction, subsequently, along with the Pelagonian nappes pile, was overthrust W-SW-ward over the carbonate Olympus-Ossa unit during the Eocene–Early Oligocene, causing a complicated nappes stacking and an important crustal thickening (D<sub>1</sub>). Subsequently, the initially ductile and progressively brittle-ductile extensional tectonics (D<sub>2</sub>) occurred during the Oligocene-Miocene causing bivergent SW-ward and NE-

ward tectonic nappes denudation and crustal thinning and uplift resulted in the final exhumation of the Ampelakia unit and the lowermost Olympos-Ossa unit as a tectonic window.

2. Today, the tectonic contacts between the several residual tectonic nappes in the Olympos-Ossa area form low-angle normal detachment faults, related to the Oligocene–Miocene extensional event, while they usually follow the old inherited structures of the thrust faults.
3. The finite strain ratios indicate that the ellipsoid is mostly flattening ( $\gamma > 1$ ), both at the western and eastern Olympos-Ossa mountainous flanks, with few deviations to near plain strain ( $\gamma = 1$ ). The estimated strain ellipsoids reveal higher deformation around or along tectonic contacts between nappes. The calculated  $W_k$  vorticity number reveals the rotational component of flow and the non-coaxial component of deformation.  $W_k$  ranges between 0.23 and 0.78 at the Olympos region, while the corresponding  $W_k$  values at the Ossa region range from 0.52 to 0.93, generally increasing at both regions from the Olympos-Ossa unit to the Pelagonian nappe. Furthermore, great  $W_k$  values were recorded within the Ampelakia unit, highlighting the suture zone between the External Hellenides carbonate Olympos-Ossa unit and the Internal Hellenides Pelagonian nappes pile.

**Supplementary Materials:** The following supporting information can be downloaded at: <https://www.mdpi.com/article/10.3390/geosciences14070179/s1>, Table S1: Summary of strain data from Pelagonian basement (KΔ 3.01-03), Ampelakia unit (KΔ 2.01- 04, KAA10-12), Flysch (KΔ 1.01-05, KΦ11) and Limestones (KA11-13) of Olympos-Ossa unit; Table S2: Summary of strain data from Pelagonian basement (KΔ 3.01-03), Ampelakia unit (KΔ 2.01- 04, KAA10-12), Flysch (KΔ 1.01-05, KΦ11) and limestones (KA11-13) of Olympos-Ossa unit; Table S3: Summary of strain data from Pelagonian basement (KΔ 3.01-03), Ampelakia unit (KΔ 2.01- 04, KAA10-12), Flysch (KΔ 1.01-05, KΦ11) and limestones (KA11-13) of Olympos-Ossa unit; Table S4: Summary of strain data from the Olympos region. Pelagonian basement (K006, 1, 2, 3, 9, 13), Ampelakia unit (8, 10, 12, OKΛ2) and limestones window (K005, OKΛ1, OK2, OKΛ3, OKΛ4); Table S5: Summary of strain data from the Olympos region. Pelagonian basement (K006, 1, 2, 3, 9, 13), Ampelakia unit (8, 10, 12, OKΛ2) and limestones window (K005, OKΛ1, OK2, OKΛ3, OKΛ4); Table S6: Summary of strain data from the Olympos region. Pelagonian basement (K006, 1, 2, 3, 9, 13), Ampelakia unit (8, 10, 12, OKΛ2) and limestones window (K005, OKΛ1, OK2, OKΛ3, OKΛ4).

**Author Contributions:** Conceptualization, I.V. and A.K.; methodology, I.V., E.K. and A.K.; software, I.V.; validation, I.V., E.K. and A.K.; formal analysis, I.V.; investigation, I.V., E.K. and A.K.; resources, I.V., I.L. and L.P.; data curation, I.V., L.P. and A.K.; writing—original draft preparation, I.V.; writing—review and editing, E.K., I.L. and A.K.; visualization, I.V.; supervision, A.K.; project administration, I.V. and A.K.; funding acquisition, I.L. and A.K. All authors have read and agreed to the published version of the manuscript.

**Funding:** This research received no external funding.

**Data Availability Statement:** The data are available in the Supplementary Materials of the present paper.

**Acknowledgments:** The authors would also like to thank three anonymous referees for their careful reviews and insightful comments and suggestions on the manuscript. The constructive suggestions of the Editors, as well as their editorial assistance, are also greatly acknowledged.

**Conflicts of Interest:** The authors declare no conflicts of interest.

## References

1. Kiliyas, A. The Alpine Geological History of the Hellenides from the Triassic to the Present—Compression vs. Extension, a Dynamic Pair for Orogen Structural Configuration: A Synthesis. *Geosciences* **2024**, *14*, 10. [[CrossRef](#)]
2. Godfriaux, I. Étude Géologique de La Région de l'Olympe (Grèce). *Ann. Geol. Pays Hell.* **1968**, *19*, 1–282.
3. Lips, A.L.W.; White, S.H.; Wijbrans, J.R. <sup>40</sup>Ar/<sup>39</sup>Ar Laserprobe Direct Dating of Discrete Deformational Events: A Continuous Record of Early Alpine Tectonics in the Pelagonian Zone, NW Aegean Area, Greece. *Tectonophysics* **1998**, *298*, 133–153. [[CrossRef](#)]
4. Kiliyas, A.; Tranos, M.; Orozco, M.; Alonso-Chaves, M.; Soto, J. Extensional Collapse of the Hellenides: A Review. *Rev. Soc. Geol. Espana* **2002**, *15*, 129–139.

5. Papapetrou, P. *Geological Map of Thessaly, 1:250.000*; Institute of Geology and Mineral Exploration (IGME): Athens, Greece, 2002.
6. Schermer, E.R. Mechanisms of Blueschist Creation and Preservation in an A-Type Subduction Zone, Mount Olympos Region, Greece. *Geology* **1990**, *18*, 1130. [[CrossRef](#)]
7. Schermer, E.R.; Lux, D.R.; Burchfiel, B.C. Temperature-time History of Subducted Continental Crust, Mount Olympos Region, Greece. *Tectonics* **1990**, *9*, 1165–1195. [[CrossRef](#)]
8. Kilias, A.; Frisch, W.; Ratschbacher, L.; Sfeikos, A. The Tectonic Evolution and P-T Conditions of Metamorphism of the “Cyano-Schists” of Eastern Thessaly (Northern/Central Greece), Greece. *Bull. Geol. Soc. Greece* **1991**, *25*, 81–99.
9. Schermer, E.R. Geometry and Kinematics of Continental Basement Deformation during the Alpine Orogeny, Mt. Olympos Region, Greece. *J. Struct. Geol.* **1993**, *15*, 571–591. [[CrossRef](#)]
10. Kilias, A. Tectonic Evolution of the Olympos—Ossa Mountain: Emplacement of the Blueschists Unit in Eastern Thessaly and Exhumation of Olympos-Ossa Carbonate Dome as a Result of Tertiary Extension (Central Greece). *Min. Wealth* **1995**, *96*, 7–22.
11. Ring, U.; Glodny, J.; Will, T.; Thomson, S. An Oligocene Extrusion Wedge of Blueschist-Facies Nappes on Evia, Aegean Sea, Greece: Implications for the Early Exhumation of High-Pressure Rocks. *J. Geol. Soc. London* **2007**, *164*, 637–652. [[CrossRef](#)]
12. Ring, U.; Will, T.; Glodny, J.; Kumerics, C.; Gessner, K.; Thomson, S.; Güngör, T.; Monié, P.; Okrusch, M.; Drüppel, K. Early Exhumation of High-pressure Rocks in Extrusion Wedges: Cycladic Blueschist Unit in the Eastern Aegean, Greece, and Turkey. *Tectonics* **2007**, *26*, TC2001. [[CrossRef](#)]
13. Xypolias, P.; Iliopoulos, I.; Chatzaras, V.; Kokkalas, S. Subduction- and Exhumation-related Structures in the Cycladic Blueschists: Insights from South Evia Island (Aegean Region, Greece). *Tectonics* **2012**, *31*, TC2001. [[CrossRef](#)]
14. Kilias, A. The Hellenides: A Multiphase Deformed Orogenic Belt, Its Structural Architecture, Kinematics and Geotectonic Setting during the Alpine Orogeny: Compression vs Extension the Dynamic Peer for the Orogen Making. A Synthesis. *J. Geol. Geosci.* **2021**, *5*, 1–56.
15. Ring, U.; Glodny, J. No Need for Lithospheric Extension for Exhuming (U)HP Rocks by Normal Faulting. *J. Geol. Soc. Lond.* **2010**, *167*, 225–228. [[CrossRef](#)]
16. Faupl, P.; Petrakakis, K.; Migiros, G.; Pavlopoulos, A. Detrital Blue Amphiboles from the Western Othrys Mountain and Their Relationship to the Blueschist Terrains of the Hellenides (Greece). *Int. J. Earth Sci.* **2002**, *91*, 433–444. [[CrossRef](#)]
17. Hinshaw, E.R.; Stockli, D.F.; Soukis, K. Zircon and Apatite U-Pb Constraints on the Tectonic Affinity and Metamorphic History of the Blueschist-Facies Ambelakia Unit, Mt. Ossa, Greece. *Tectonics* **2023**, *42*, e2022TC007608. [[CrossRef](#)]
18. Barnes, C.J.; Zack, T.; Bułka, M.; Rösel, D.; Mark, C.; Schneider, D.A. Dating Metamorphic Processes and Identifying 87Sr/86Sr Inheritance Using Volume-Coupled Rb/Sr Geochronology and Geochemistry of in Situ White Mica: A Demonstration with HP/LT Rocks from Syros, Greece. *Chem. Geol.* **2024**, *660*, 122149. [[CrossRef](#)]
19. Lister, G.S.; Forster, M.A. White Mica 40Ar/39Ar Age Spectra and the Timing of Multiple Episodes of High-pressure Metamorphic Mineral Growth in the Cycladic Eclogite–Blueschist Belt, Syros, Aegean Sea, Greece. *J. Metamorph. Geol.* **2016**, *34*, 401–421. [[CrossRef](#)]
20. Barton, C.M. The Tectonic Vector and Emplacement Age of an Allochthonous Basement Slice in the Olympos Area, N.E. Greece. *Bull. Société Géologique Fr.* **1976**, *S7-XVIII*, 253–258. [[CrossRef](#)]
21. Doutsos, T.; Pe-Piper, G.; Boronkay, K.; Koukouvelas, I. Kinematics of the Central Hellenides. *Tectonics* **1993**, *12*, 936–953. [[CrossRef](#)]
22. Xypolias, P.; Kokkalas, S.; Skourlis, K. Upward Extrusion and Subsequent Transpression as a Possible Mechanism for the Exhumation of HP/LT Rocks in Evia Island (Aegean Sea, Greece). *J. Geodyn.* **2003**, *35*, 303–332. [[CrossRef](#)]
23. Chatzaras, V.; Xypolias, P.; Kokkalas, S.; Koukouvelas, I. Oligocene–Miocene Thrusting in Central Aegean: Insights from the Cycladic Island of Amorgos. *Geol. J.* **2011**, *46*, 619–636. [[CrossRef](#)]
24. Aravadinou, E.; Xypolias, P.; Chatzaras, V.; Iliopoulos, I.; Gerogiannis, N. Ductile Nappe Stacking and Refolding in the Cycladic Blueschist Unit: Insights from Sifnos Island (South Aegean Sea). *Int. J. Earth Sci.* **2016**, *105*, 2075–2096. [[CrossRef](#)]
25. Gerogiannis, N.; Xypolias, P. Retroward Extrusion of High-pressure Rocks: An Example from the Hellenides (Pelion Blueschist Nappe, NW Aegean). *Terra Nova* **2017**, *29*, 372–381. [[CrossRef](#)]
26. Kilias, A.; Thomaidou, E.; Katrivanos, E.; Vamvaka, A.; Fassoulas, C.; Pipera, K.; Falalakis, G.; Avgerinas, S.; Sfeikos, A. A Geological Cross-Section through Northern Greece from Pindos to Rhodope Mountain Ranges: A Field Guide across the External and Internal Hellenides. *J. Virtual Explor.* **2016**, *50*, 1–107.
27. Ring, U.; Brandon, M.T.; Lister, G.S.; Willett, S.D. *Exhumation Processes: Normal Faulting, Ductile Flow & Erosion*; GSL Special Publications: London, UK, 1999.
28. Shaked, Y.; Avigad, D.; Garfunkel, Z. Alpine High-Pressure Metamorphism at the Almyropotamos Window (Southern Evia, Greece). *Geol. Mag.* **2000**, *137*, 367–380. [[CrossRef](#)]
29. McKenzie, D. Active Tectonics of the Mediterranean Region. *Geophys. J. Int.* **1972**, *30*, 109–185. [[CrossRef](#)]
30. Taymaz, T.; Jackson, J.; McKenzie, D. Active Tectonics of the North and Central Aegean Sea. *Geophys. J. Int.* **1991**, *106*, 433–490. [[CrossRef](#)]
31. Jolivet, L.; Faccenna, C.; Huet, B.; Labrousse, L.; Le Pourhiet, L.; Lacombe, O.; Lecomte, E.; Burov, E.; Denèle, Y.; Brun, J.P.; et al. Aegean Tectonics: Strain Localisation, Slab Tearing and Trench Retreat. *Tectonophysics* **2013**, *597–598*, 1–33. [[CrossRef](#)]
32. Lazos, I.; Pikridas, C.; Chatzipetros, A.; Pavlides, S. Determination of Local Active Tectonics Regime in Central and Northern Greece, Using Primary Geodetic Data. *Appl. Geomat.* **2021**, *13*, 3–17. [[CrossRef](#)]

33. Brun, J.P.; Faccenna, C. Exhumation of High-Pressure Rocks Driven by Slab Rollback. *Earth Planet Sci. Lett.* **2008**, *272*, 1–7. [[CrossRef](#)]
34. Lazos, I.; Sboras, S.; Pikridas, C. Tectonic Geodesy Synthesis and Review of the North Aegean Region, Based on the Strain Patterns of the North Aegean Sea, Strymon Basin and Thessalian Basin Case Studies. *Appl. Sci.* **2023**, *13*, 9943. [[CrossRef](#)]
35. Erman, C.; Yolsal-Çevikbilen, S.; Eken, T.; Tilmann, F.; Keleş, D.; Taymaz, T. Constraints on the Lithospheric Kinematics in the Aegean and Western Anatolia Unveiled by SKS Splitting Observations. *J. Geophys. Res. Solid Earth* **2022**, *127*, e2022JB025265. [[CrossRef](#)]
36. Taymaz, T.; Yilmaz, Y.; Dilek, Y. The Geodynamics of the Aegean and Anatolia: Introduction. *Geol. Soc. Spec. Publ.* **2007**, *291*, 1–16. [[CrossRef](#)]
37. McKenzie, D.; Jackson, J. Conditions for Flow in the Continental Crust. *Tectonics* **2002**, *21*, 5–1–5–7. [[CrossRef](#)]
38. Jolivet, L.; Menant, A.; Clerc, C.; Sternai, P.; Bellahsen, N.; Leroy, S.; Pik, R.; Stab, M.; Faccenna, C.; Gorini, C. Extensional Crustal Tectonics and Crust-Mantle Coupling, a View from the Geological Record. *Earth Sci. Rev.* **2018**, *185*, 1187–1209. [[CrossRef](#)]
39. Lazos, I.; Chatzipetros, A.; Pavlides, S.; Pikridas, C.; Bitharis, S. Tectonic Crustal Deformation of Corinth Gulf, Greece, Based on Primary Geodetic Data. *Acta Geodyn. Geomater.* **2020**, *17*, 413–424. [[CrossRef](#)]
40. Robertson, A.H.F.; Dixon, J.E.; Brown, S.; Collins, A.; Morris, A.; Pickett, E.; Sharp, I.; Ustaömer, T. Alternative Tectonic Models for the Late Palaeozoic–Early Tertiary Development of Tethys in the Eastern Mediterranean Region. *Geol. Soc. Spec. Publ.* **1996**, *105*, 239–263. [[CrossRef](#)]
41. Gawlick, H.-J.; Frisch, W.; Hoxha, L.; Dumitrica, P.; Krystyn, L.; Lein, R.; Missoni, S.; Schlagintweit, F. Mirdita Zone Ophiolites and Associated Sediments in Albania Reveal Neotethys Ocean Origin. *Int. J. Earth Sci.* **2008**, *97*, 865–881. [[CrossRef](#)]
42. Gawlick, H.J.; Missoni, S.; Schlagintweit, F.; Suzuki, H.; Frisch, W.; Krystyn, L.; Blau, J.; Lein, R. Jurassic Tectonostratigraphy of the Austroalpine Domain. *J. Alp. Geol.* **2009**, *50*, 1–152.
43. Robertson, A. Late Palaeozoic–Cenozoic Tectonic Development of Greece and Albania in the Context of Alternative Reconstructions of Tethys in the Eastern Mediterranean Region. *Int. Geol. Rev.* **2012**, *54*, 373–454. [[CrossRef](#)]
44. Robertson, A.H.F.; Trivić, B.; Đerić, N.; Bucur, I.I. Tectonic Development of the Vardar Ocean and Its Margins: Evidence from the Republic of Macedonia and Greek Macedonia. *Tectonophysics* **2013**, *595–596*, 25–54. [[CrossRef](#)]
45. Kostaki, G.; Gawlick, H.-J.; Missoni, S.; Kiliyas, A.; Katrivanos, E. New Stratigraphic and Palaeontological Data from Carbonates Related to the Vourinos–Pindos Ophiolite Emplacement: Implications for the Provenance of the Ophiolites (Hellenides). *J. Geol. Soc. Lond.* **2024**, *181*, jgs2023–jgs2127. [[CrossRef](#)]
46. Yarwood, G.A.; Aftalion, M. Field Relations and U–Pb Geochronology of a Granite from the Pelagonian Zone of the Hellenides (High Pieira, Greece). *Bull. Société Géologique Fr.* **1976**, *S7–XVIII*, 259–264. [[CrossRef](#)]
47. Mountrakis, D.; Sapountzis, E.; Kiliyas, A.; Eleftheriadis, G.; Christofides, G. Paleogeographic Conditions in the Western Pelagonian Margin in Greece during the Initial Rifting of the Continental Area. *Can. J. Earth Sci.* **1983**, *20*, 1673–1681. [[CrossRef](#)]
48. Mountrakis, D. The Pelagonian Zone in Greece: A Polyphase-Deformed Fragment of the Cimmerian Continent and Its Role in the Geotectonic Evolution of the Eastern Mediterranean. *J. Geol.* **1986**, *94*, 335–347. [[CrossRef](#)]
49. Pe-Piper, G.; Doutsos, T.; Mijara, A. Petrology and Regional Significance of the Hercynian Granitoid Rocks of the Olympiada Area, Northern Thessaly, Greece. *Chem. Erde-Geochem.* **1993**, *53*, 21–36.
50. Kiliyas, A.; Frisch, W.; Avgerinas, A.; Dunkl, I.; Falalakis, G.; Gawlick, H.-J. Alpine Architecture and Kinematics of Deformation of the Northern Pelagonian Nappe Pile in the Hellenides. *Austrian J. Earth Sci.* **2010**, *103*, 4–28.
51. Most, T.; Frisch, W.; Dunkl, I.; Kadosa, B.; Boev, B.; Avgerinas, A.; Kiliyas, A. Geochronological and Structural Investigations of the Northern Pelagonian Crystalline Zone. Constraints from K/Ar and Zircon and Apatite Fission Track Dating. *Bull. Geol. Soc. Greece* **2001**, *34*, 91. [[CrossRef](#)]
52. Katrivanos, E.; Kiliyas, A.; Mountrakis, D. Kinematics of Deformation and Structural Evolution of the Paikon Massif (Central Macedonia, Greece): A Pelagonian Tectonic Window? *Neues Jahrb. Geol. Palaontol. Abh.* **2013**, *269*, 149–171. [[CrossRef](#)]
53. Tsagkalidis, A. Petrological Study of the Ossa Region of Thessaly. Ph.D. Thesis, Agricultural University of Athens, Athens, Greece, 1990.
54. Nance, D. Tectonic History of a Segment of the Pelagonian Zone, Northeastern Greece. *Can. J. Earth Sci.* **1981**, *18*, 1111–1126. [[CrossRef](#)]
55. Kiliyas, A. Transpression Tectonics of the Central Hellenides Changing of the Translation Paths Due to the Transpression (North-Central Greece). *Neues Jahrb. Geol. Paläontologie-Monatshefte* **1991**, *1991*, 291–306. [[CrossRef](#)]
56. Ramsay, O.; Huber, I. *The Techniques of Modern Structural Geology: Strain Analysis*; Academic Press: Cambridge, MA, USA, 1983; Volume 1.
57. Ramsay, O.; Huber, I. *The Techniques of Modern Structural Geology: Folds and Fractures*; Academic Press: Cambridge, MA, USA, 1987; Volume 2.
58. Passchier, C.W.; Trouw, R.A.J. *Microtectonics*; Springer: Berlin/Heidelberg, Germany, 1996; ISBN 3-540-64003-7.
59. Kassem, O.M. Finite-Strain Analysis in Orthogneiss of the Gran Paradiso Massif. Ph.D. Thesis, Johannes Gutenberg-Universität, Mainz, Germany, 2005.
60. Fry, N. Random Point Distributions and Strain Measurement in Rocks. *Tectonophysics* **1979**, *60*, 89–105. [[CrossRef](#)]
61. Panozzo, R. Two-Dimensional Strain from the Orientation of Lines in a Plane. *J. Struct. Geol.* **1984**, *6*, 215–221. [[CrossRef](#)]
62. Wallbrecher, E. “Fabric 8” Geological Software 1986.

63. Flinn, D. On Folding During Three-Dimensional Progressive Deformation. *Q. J. Geol. Soc.* **1962**, *118*, 385–428. [[CrossRef](#)]
64. Hossack, J.R. Pebble Deformation and Thrusting in the Bygdin Area (Southern Norway). *Tectonophysics* **1968**, *5*, 315–339. [[CrossRef](#)]
65. Katsikatos, G.; Migiros, G. *Geological Map of Greece, Rapsani Sheet, 1:50.000*; Institute of Geology and Mineral Exploration (IGME): Athens, Greece, 1987.
66. Röller, K.; Trepmann, C. *Stereo 32*, version 1.0.1; Ruhr-Universität Bochum, Institut für Geologie, Mineralogie & Geophysik: Bochum, Germany, 2003.
67. Röller, K.; Trepmann, C. *Stereo 32*, 1.0.1; Ruhr-Universität Bochum, Institut für Geologie, Mineralogie & Geophysik: Bochum, Germany, 2008.
68. Dunnet, D. A Technique of Finite Strain Analysis Using Elliptical Particles. *Tectonophysics* **1969**, *7*, 117–136. [[CrossRef](#)]
69. Lisle, R.J. *Geological Strain Analysis. A Manual for the Rf/φ Method*; Pergamon Press: New York, NY, USA, 1985.
70. Erslev, E.A. Normalized Center-to-Center Strain Analysis of Packed Aggregates. *J. Struct. Geol.* **1988**, *10*, 201–209. [[CrossRef](#)]
71. Erslev, E.A.; Ge, H. Least-Squares Center-to-Center and Mean Object Ellipse Fabric Analysis. *J. Struct. Geol.* **1990**, *12*, 1047–1059. [[CrossRef](#)]
72. Katsivrias, N.; Triantaphyllis, E. *Geological Map of Greece, Livadhion Sheet, 1:50.000*; Institute of Geology and Mineral Exploration (IGME): Athens, Greece, 1988.
73. Panozzo, R.H. Two-Dimensional Analysis of Shape-Fabric Using Projections of Digitized Lines in a Plane. *Tectonophysics* **1983**, *95*, 279–294. [[CrossRef](#)]
74. Lister, G.S. Discussion: Crossed-Girdle c-Axis Fabrics in Quartzites Plastically Deformed by Plane Strain and Progressive Simple Shear. *Tectonophysics* **1977**, *39*, 51–54. [[CrossRef](#)]
75. Migiros, G. *Geological Map of Greece, Gonni Sheet, 1:50.000*; Institute of Geology and Mineral Exploration (IGME): Athens, Greece, 1985.
76. Wallis, S.R. Vorticity Analysis in a Metachert from the Sanbagawa Belt, SW Japan. *J. Struct. Geol.* **1992**, *14*, 271–280. [[CrossRef](#)]
77. Wallis, S. Vorticity Analysis and Recognition of Ductile Extension in the Sanbagawa Belt, SW Japan. *J. Struct. Geol.* **1995**, *17*, 1077–1093. [[CrossRef](#)]
78. Xypolias, P. Vorticity Analysis in Shear Zones: A Review of Methods and Applications. *J. Struct. Geol.* **2010**, *32*, 2072–2092. [[CrossRef](#)]
79. Law, R.D.; Knipe, R.J.; Dayan, H. Strain Path Partitioning within Thrust Sheets: Microstructural and Petrofabric Evidence from the Moine Thrust Zone at Loch Eriboll, Northwest Scotland. *J. Struct. Geol.* **1984**, *6*, 477–497. [[CrossRef](#)]
80. Platt, J.P.; Behrmann, J.H. Structures and Fabrics in a Crustal-Scale Shear Zone, Betic Cordillera, SE Spain. *J. Struct. Geol.* **1986**, *8*, 15–33. [[CrossRef](#)]
81. Schmid, S.M.; Casey, M. Complete Fabric Analysis of Some Commonly Observed Quartz C-Axis Patterns. *Miner. Rock Deform. Lab. Stud.* **1986**, *36*, 263–286.
82. Vissers, R.L.M. Asymmetric Quartz C-Axis Fabrics and Flow Vorticity: A Study Using Rotated Garnets. *J. Struct. Geol.* **1989**, *11*, 231–244. [[CrossRef](#)]
83. Law, R.D. Crystallographic Fabrics: A Selective Review of Their Applications to Research in Structural Geology. *Geol. Soc. Lond. Spec. Publ.* **1990**, *54*, 335–352. [[CrossRef](#)]
84. Wernicke, B. Low-Angle Normal Faults in the Basin and Range Province: Nappe Tectonics in an Extending Orogen. *Nature* **1981**, *291*, 645–648. [[CrossRef](#)]
85. Dewey, J.F. Extensional Collapse of Orogens. *Tectonics* **1988**, *7*, 1123–1139. [[CrossRef](#)]
86. Gautier, P.; Brun, J.-P. Ductile Crust Exhumation and Extensional Detachments in the Central Aegean (Cyclades and Evvia Islands). *Geodin. Acta* **1994**, *7*, 57–85. [[CrossRef](#)]

**Disclaimer/Publisher’s Note:** The statements, opinions and data contained in all publications are solely those of the individual author(s) and contributor(s) and not of MDPI and/or the editor(s). MDPI and/or the editor(s) disclaim responsibility for any injury to people or property resulting from any ideas, methods, instructions or products referred to in the content.